

2

Dual-Modality Imaging: More Than the Sum of its Components

B.H. HASEGAWA* AND H. ZAIDI†

1. Introduction

The field of diagnostic radiology encompasses a wealth of imaging techniques that now are essential for evaluating and managing patients who need medical care. Traditional imaging methods such as plain film radiography and more recent techniques such as x-ray computed tomography (CT) and magnetic resonance imaging (MRI) can be used to evaluate a patient's anatomy with submillimeter spatial resolution to discern structural abnormalities and to evaluate the location and extent of disease. These methods also offer relatively fast scan times, precise statistical characteristics, and good tissue contrast especially when contrast media are administered to the patient. In addition, x-ray fluoroscopy and angiography can be used to evaluate the patency of blood vessels, the mechanical performance of the cardiovascular system, and structural abnormalities in the gastrointestinal or genitourinary systems. Similarly, CT and MRI can be performed with cardiac gating to the heart at different phases of the cardiac cycle. Computed tomography recently has experienced a significant increase in utilization with the advent of multislice helical scanning techniques that cover a large region of the patient's anatomy within a single breath-hold, with scan speeds that can capture both the arterial and venous phases of the contrast bolus. These increased scan speeds also enhance patient comfort, and contribute to patient throughput and cost effectiveness.

X-ray projection imaging, computed tomography, and magnetic resonance imaging differentiate disease from normal tissue by revealing structural differences or differences in regional perfusion of the administered contrast media. The interpretation of the images can be complicated when normal perfusion patterns are disrupted by prior surgery or radiation therapy, which can lead to tissue damage or necrosis where contrast patterns can mimic

*Prof. B.H. Hasegawa, Department of Radiology, University of California, San Francisco, CA, USA

†PD Dr H. Zaidi, Geneva University Hospital, Division of Nuclear Medicine, CH-1211 Geneva, Switzerland

those associated with neoplasia. This presents a significant challenge when the imaging techniques are used to define the anatomical extent of disease as is needed for planning highly conformal radiation treatment or for planning highly targeted therapeutic regimes.

In comparison to the anatomical imaging techniques described above, functional imaging methods including planar scintigraphy, single-photon emission computed tomography (SPECT), positron emission tomography (PET), and magnetic resonance spectroscopy (MRS), assess regional differences in the biochemical status of tissues.^{1,2} In nuclear medicine, including SPECT and PET, this is done by administering the patient with a biologically active molecule or pharmaceutical which is radiolabeled and accumulated in response to its biochemical attributes. Radionuclide imaging and nuclear medicine rely on the tracer principle in which a minute amount of a radiopharmaceutical is administered to assess physiological function or the biomolecular status of a tissue, tumour, or organ within the patient. The amount of the radiopharmaceutical is sufficiently small so that its administration does not perturb the normal function of the patient. However, the radiopharmaceutical produces a radioactive signal that can be measured, and ideally imaged, using an external array of radiation detectors. By design, the radiopharmaceutical has a targeted action, allowing it to be imaged to evaluate specific physiological processes in the body. There now are many radiopharmaceuticals available for medical diagnosis, with additional radiotracers available for *in vivo* as well as *in vitro* biological experimentation.

Nuclear medicine relies on use of radionuclide tracers which emit radiation in amounts proportional to their regional concentration within the body. For this reason, radionuclide imaging often is called “emission” imaging. This is in contrast to x-ray or “transmission” imaging where an external radiation source transmits radiation through the body and onto a set of opposing detectors. The properties of emission imaging are best suited for imaging functional processes, while transmission imaging is best suited for visualizing anatomical structure. Because the amount of radiation that can be administered internally to the patient is limited by considerations of radiation dose and count rate, radionuclide images inherently have poor photon statistics, are produced with only modest spatial resolution, and require relatively long scan times. In addition, the visual quality of radionuclide images can be degraded by physical factors such as photon attenuation and scatter radiation.³⁻¹⁰ In contrast, transmission images are produced with short scan times, excellent signal-to-noise characteristics, and submillimeter spatial resolution, but generally contain limited functional information. These considerations illustrate that x-ray (transmission) and radionuclide (emission) imaging provide quite different but complementary information about the patient.¹¹⁻¹⁴ This information can be interpreted by the diagnostician to detect, localize, and diagnose diseases. Similarly, biomedical research scientists can analyze these attributes to monitor and measure processes that are important for

biological research, drug discovery, and development of new diagnostic and therapeutic techniques in humans and animals.

Several investigators have developed methods which attempt to improve the correlation between anatomical and physiological information obtained using these x-ray transmission and radionuclide emission imaging studies. Software-based image registration¹⁵⁻¹⁷ can fuse images from two or more different studies after they are acquired separately. Commonly, image registration techniques produce a single “fused” or “combined” image in which, for example, the radionuclide distribution is displayed in colour over a grey-scale CT image of the same anatomical region. The simplest form of image registration uses “rigid-body” translation and rotation to match the two image data sets. These techniques can be applied most successfully to neurological studies,^{18,19} where the skull provides a rigid structure that maintains the geometrical relationship of structures within the brain. The situation is more complicated when image registration techniques are applied to other areas of the body, for example the thorax and abdomen, where the body can bend and flex, especially when the x-ray and radionuclide data are captured using different machines in separate procedures, often on different days (see chapter 9). Geometrical relationships between different anatomical regions can be affected by the shape of the patient table, the orientation of the body and limbs during the imaging procedure, and the respiratory state of the patient.²⁰ In these cases, image registration might match the patient anatomy in one region of the body, but not in all anatomical regions. Image warping can improve registration over a larger region of the patient’s anatomy, but in most cases, software-based image registration can be challenging and, at most institutions, is not used routinely for clinical procedures.^{16,17}

With the goal of improving the correlation of different types of image data, other investigators have developed instrumentation which integrate both x-ray and radionuclide imaging in a single device.^{1,21-35} This technique, often called dual-modality imaging, can combine a PET or SPECT system with a CT scanner, using a common patient table, computer, and gantry so that both the x-ray and radionuclide image data are acquired sequentially without removing the patient from the scanner. This technique thereby produces anatomical and functional images with the patient in the same position and during a single procedure, which simplifies the image registration and fusion processes.^{1,25,28,32,34,36} In seeking to achieve accurate registration of the anatomical and functional data, dual-modality imaging offers several potential advantages over conventional imaging techniques.³⁷ First, the radionuclide and x-ray images are supplementary and complementary. Radionuclide data can identify areas of disease that are not apparent on the x-ray images alone.^{14,38-41} X-ray images provide an anatomical context that interpreters use to differentiate normal radionuclide uptake from that indicating disease, and to help localize disease sites within the body. Second, the x-ray data can be used to generate a patient-specific map of attenuation coefficients and other *a priori* anatomical data which in turn is

used to correct the radionuclide data for errors due to photon attenuation, scatter radiation, and other physical effects.^{1,21,22,25,27,42-44} In these ways, the x-ray data can be used to improve both the visual quality and the quantitative accuracy of the correlated radionuclide data.

2. Brief History of Dual-Modality Imaging

Whereas the advent of dedicated dual-modality imaging systems designed specifically for clinical use is relatively recent, the potential advantages of combining anatomical and functional imaging has been recognized for several decades by radiological scientists and physicians. Many of the pioneers of nuclear medicine, including Mayneord,⁴⁵⁻⁴⁷ Anger,^{48,49} Cameron and Sorenson,⁵⁰ and Kuhl⁵¹ recognized that a radionuclide imaging system could be augmented by adding an external radioisotope source to acquire transmission data for anatomical correlation of the emission image. Furthermore, Kuhl *et al.*⁵² added an external radionuclide source on his Mark IV brain scanner to produce anatomical images useful for both localizing regions of radionuclide uptake and to correct for soft tissue absorption in the radionuclide emission data. In a 1974 review of photon attenuation, Budinger and Gullberg⁵³ noted that a patient-specific attenuation map could be produced from transmission data acquired using an external radionuclide source or extracted from a spatially correlated CT scan of the patient. A specific implementation of a combined emission-transmission scanner was disclosed by Mirshanov⁵⁴ who produced an engineering concept diagram showing a semiconductor detector to record radionuclide emission data and a strip scintillator to record coregistered x-ray transmission data from a patient (Figure 1). In addition, Kaplan *et al.*⁵⁵ proposed a high performance scintillation camera to record both emission data from an internal radionuclide source and transmission data from an external x-ray source. However these concepts were never reduced to practice or implemented in either an experimental or a clinical setting.⁵⁶

In late 1980's and early 1990's, Hasegawa *et al.*^{23,26,57,58} at the University of California, San Francisco, pioneered the development of dedicated emission/transmission imaging systems which could record both radionuclide and x-ray data for correlated functional/structural imaging. The first prototype, developed by Lang *et al.*^{26,58} used an array of HPGe detectors (Figure 2) with sufficient energy discrimination and count-rate performance to discriminate γ -rays emitted by an internally distributed radiopharmaceutical from x-rays transmitted through the body from an external x-ray source. Phantom experiments with this first prototype led to the development of a second prototype (Figure 3) having a 20-cm reconstruction diameter that could record emission and transmission data from stationary animal or object using a single HPGe detector array. Kalki *et al.*^{59,60} used this second prototype in animal studies both to demonstrate the capability of the system to facilitate image correlation and to test the feasibility of correcting the

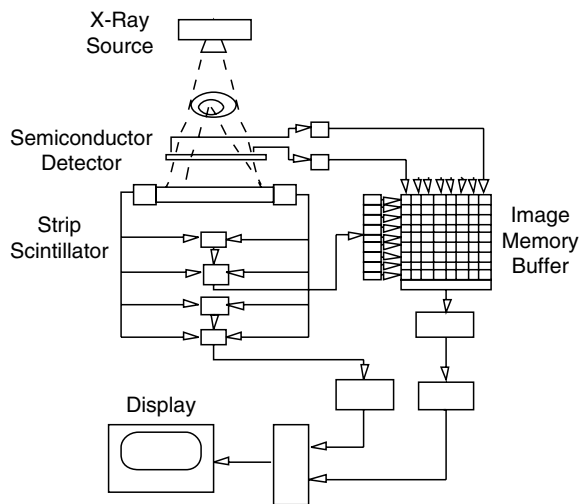


FIGURE 1. Concept drawing of transmission-emission tomography system proposed in the Soviet Union in 1987. System includes semiconductor detector for radionuclide imaging and strip scintillator for x-ray imaging, with electronics for combined recording and display of x-ray and radionuclide data sets. Reprinted from ref.⁵⁴

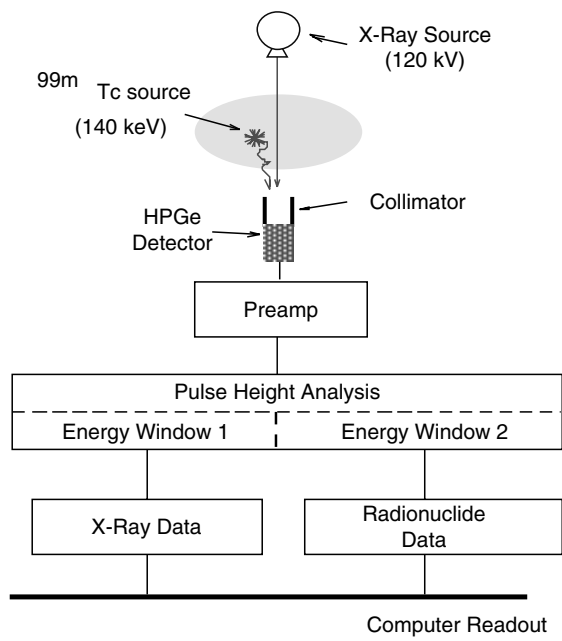


FIGURE 2. Schematic of data acquisition of combined emission-transmission imaging system developed at UCSF using single high-purity germanium detector array with fast pulse-counting electronics for simultaneous emission-transmission imaging.

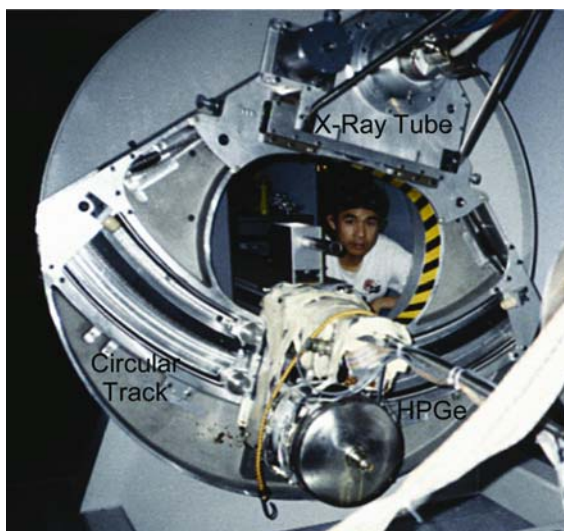


FIGURE 3. Early emission-transmission CT system at UCSF had an HPGe detector was translated across a circular arc to simulate an entire detector array and was rotated around an isocenter for tomographic imaging. Detector was read-out using fast pulse-counting electronics (Figure 2) using energy discrimination to separate the simultaneously acquired x-ray and radionuclide data. Reprinted with permission from ref.¹

radionuclide data for photon attenuation using coregistered x-ray transmission data. Because the HPGe detector implemented in these first two prototypes was expensive and impractical for clinical use, the UCSF group next implemented a SPECT/CT scanner (Figure 4) for patient studies by sitting a GE 9800 Quick CT scanner in tandem with a GE 400 XR/T SPECT system.^{21,22,42} This configuration allowed the patient to remain on a common patient table for radionuclide and x-ray imaging with separate detector technologies that already had been optimized for clinical use both in terms of technical performance and cost-effectiveness. The investigators used this system to demonstrate that CT data could produce a patient-specific attenuation map that could be incorporated into an iterative reconstruction algorithm for attenuation correction of the correlated radionuclide data. The system was used for imaging studies with phantoms, animals, and patients and demonstrated that the use of combined emission and transmission data could improve both the visual quality and the quantitative accuracy of radionuclide data in comparison to SPECT data alone.^{21,22,42}

The first integrated PET/CT system (Figure 5) was developed by Townsend and co-workers at the University of Pittsburgh in 1998^{28,33-35} by combining the imaging chains from a Somatom AR.SP (Siemens Medical Systems) CT system with an ECAT ART (CTI/Siemens) PET scanner. Both

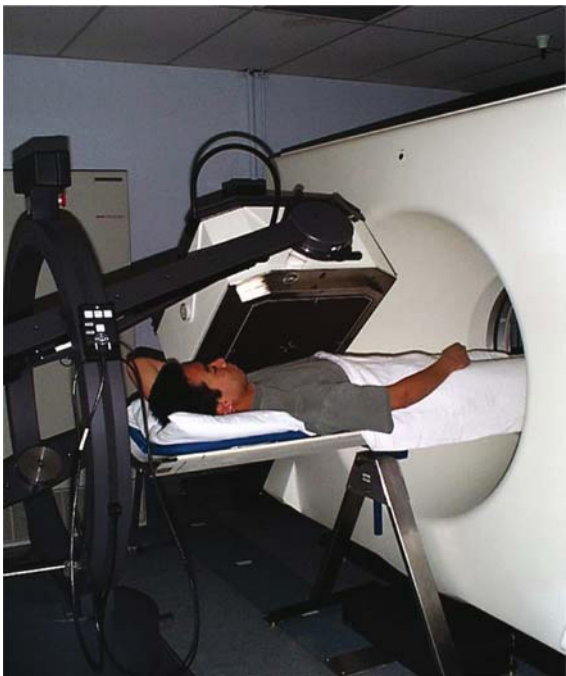


FIGURE 4. Combined SPECT/CT system configured at UCSF from a GE 9800 CT Quick CT scanner and a 400 XR/T SPECT system with a common patient table to translate the patient between the reconstruction volumes of the CT and SPECT systems. Reprinted with permission from ref.¹

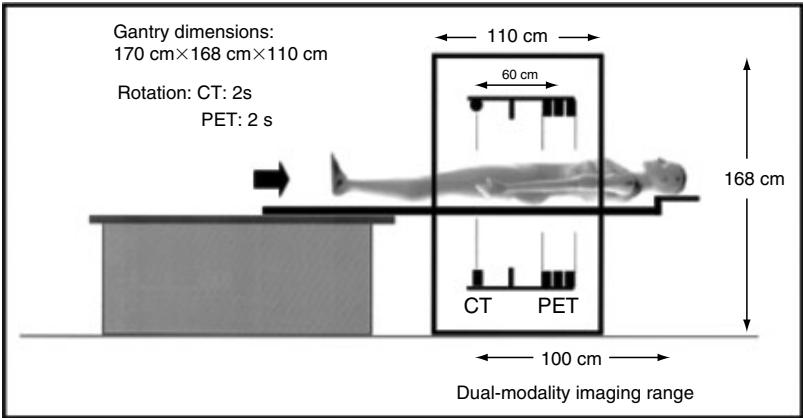


FIGURE 5. Schematic of combined PET/CT scanner developed at University of Pittsburgh by Townsend and co-workers. PET components were mounted on back of rotating CT scanner assembly. Centers of fields-of-view between PET and CT (vertical lines) were 60 cm apart. Combined PET/CT gantry was 110 cm deep, 170 cm high, and 168 cm wide. PET and CT data were acquired over 100 cm axial range of patient. Reprinted with permission from ref.³⁵

the CT components and the PET detectors were mounted on opposite sides of the rotating stage of the CT system, and imaged a patient with a common patient table translated between the centers of the two tomographs which are offset axially by 60 cm.³³ The PET/CT prototype was operational at the University of Pittsburgh from May 1998 to August 2001, during which over 300 cancer patients were scanned. The success of these initial studies prompted significant interest from the major medical imaging equipment manufacturers who now all have introduced commercial PET/CT scanners for clinical use.

In 1999 and 2000, SPECT/CT and PET/CT dual-modality imaging systems were introduced by the major medical equipment manufacturers for clinical use, with approximately 400 systems of each type sold by midyear 2004. A significant success of PET/CT has been the improved image quality of FDG images for tumour localization.^{38,39,41,61} The major use of SPECT/CT has been in reducing attenuation artefacts and improving the quality of myocardial perfusion imaging with ^{99m}Tc-sestamibi.^{21,59,62-64} SPECT/CT also has demonstrated advantages for oncologic imaging with single-photon agents.^{12,25,40,41,65-70} Both SPECT/CT and PET/CT have demonstrated their ability to facilitate attenuation correction using an x-ray based patient-specific attenuation map that can be produced faster and more accurately than attenuation maps generated with external radionuclide sources.^{10,34} Clinical studies are underway to evaluate the applicability of x-ray based correction of photon attenuation,⁷¹ and early results demonstrate improvement in sensitivity, specificity, and predictive accuracy in comparison to SPECT perfusion studies reconstructed without correction for photon attenuation. The anatomical information from PET/CT improves the differentiation of physiological (normal) uptake of FDG and other radiopharmaceuticals from that associated with disease, and thereby can reduce false positive errors in comparison to lesion characterization when radionuclide imaging is used alone. By providing high-resolution anatomical information from CT, dual-modality imaging also correlates functional and anatomical data to improve disease localization^{14,38,39,41,61} and facilitates treatment planning for radiation oncology^{12,72} or surgery.^{68,73,74}

3. Capabilities of Dual-Modality Imaging

Dual-modality techniques offer a critical advantage over separate CT and radionuclide imaging systems in correlating functional and anatomical images without moving the patient (other than table translation). Dual-modality imaging also can account consistently for differences in reconstruction diameter, offsets in isocenter, image reconstruction coordinates, and image format (e.g., 512×512 vs. 128×128) between the CT and radionuclide image geometries to perform image coregistration and image fusion. Depending on the design of the system, image registration software also may be

needed to account for table sag or for misalignment when the patient moves between the CT and radionuclide image scans. Generally, the coordinate systems implicit in the radionuclide and CT image geometries are calibrated with respect to each other using fiducial markers that are scanned with both CT and radionuclide imaging. The image registration must be confirmed to avoid misregistration errors in the dual-modality images or in the radionuclide image reconstructed using CT-derived attenuation maps.

Dual-modality imaging also provides *a priori* patient-specific information that is needed to correct the radionuclide data for photon attenuation and other physical effects. Increasingly, x-ray sources are replacing external radionuclide sources for acquisition of the “transmission scan” to obtain projection data which can be reconstructed to produce a patient-specific map of linear attenuation coefficients so that the radionuclide (SPECT or PET) data can be reconstructed with a correction for photon attenuation.^{5,75-80} Because the external radionuclide sources produce a limited fluence rate, the transmission scans often require several minutes and produce images that are noisy and photon-limited. Alternatively, transmission data can be acquired using an x-ray source having a small focus, a significantly higher photon fluence rate than a radionuclide source, and therefore produce tomographic reconstructions with 1 mm (or better spatial resolution) with excellent noise characteristics. The resulting CT images then can be calibrated to produce a patient-specific map of linear attenuation coefficients calculated for the energy of the radionuclide photons.^{21-23,29,34,42-44} In this way, the CT data from a dual-modality imaging system facilitates, and in some ways simplifies, the process of correcting the radionuclide image for photon attenuation.

Several different CT-based attenuation correction techniques have been developed^{21-23,29,34,42-44} and are reviewed in chapter 6. As an example, the technique developed by Blankespoor *et al.*^{22,81} obtains CT calibration measurements from a phantom with cylindrical inserts containing water, fat-equivalent (ethanol), and bone equivalent material (K_2HPO_4). CT numbers extracted from each region are plotted against their known attenuation coefficients at the photon energy of the radionuclide to provide a piecewise linear calibration curve.^{22,82,83} During the dual-modality imaging study, both CT and radionuclide data of the patient are acquired. The calibration curve described above is used to convert the CT image of the patient into an object-specific attenuation map. The resulting attenuation map then can be incorporated into the reconstruction of the radionuclide data⁸⁴ using ML-EM or other iterative algorithm, to correct the radionuclide data for perturbations due to photon attenuation. This or a similar process can be used to improve both the image quality and the quantitative accuracy of SPECT or PET images (see chapter 4). Important clinical applications include attenuation correction of myocardial perfusion images^{80,85} to resolve false-positive defects caused by soft-tissue attenuation (Figure 6). In addition, the visual quality of oncologic images can be significantly improved when the ¹⁸F-FDG data are reconstructed using attenuation correction.

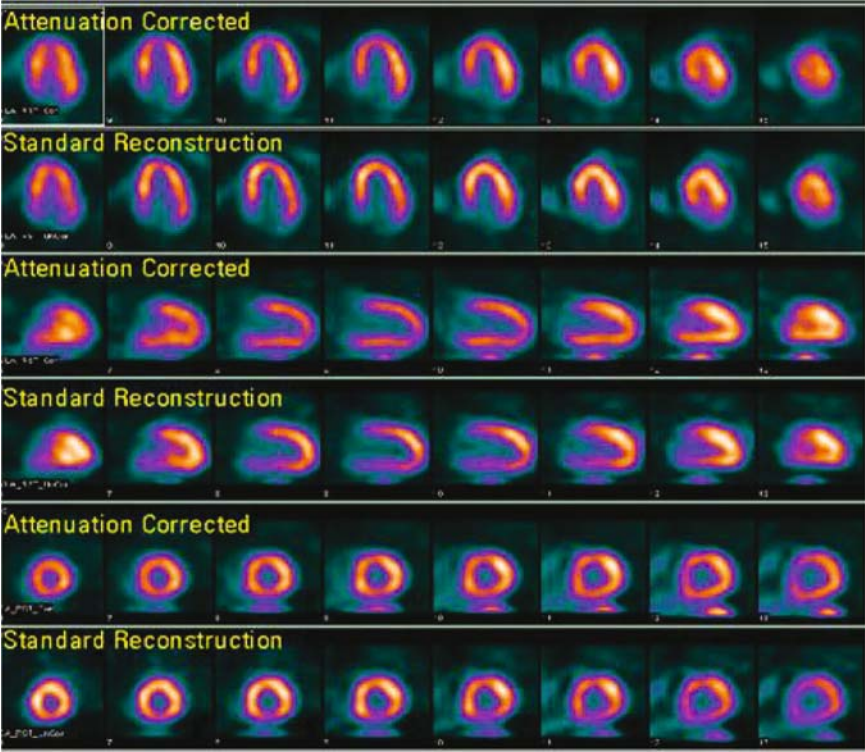


FIGURE 6. Myocardial perfusion scans acquired with GE Discovery VG using x-ray derived attenuation map. In each pair of rows, the top and bottom rows represent data reconstructed with and without attenuation correction respectively. In this study, the patient presented with chest pain with borderline normal ejection fraction of 47%. Resting ^{99m}Tc -sestamibi perfusion scan without attenuation correction shows mild inferior wall defect. However, myocardial perfusion images appear normal when reconstructed with x-ray based attenuation correction. Reprinted with permission from GE Healthcare Technologies, Waukesha, WI.

In addition to the energy conversion process described above, it is important to match the geometric characteristics of the CT-derived attenuation map and radionuclide tomograms. This typically requires the CT data to be resampled so that it can be presented in slices that have the same pixel format (e.g. 128×128 , or 256×256) and same slice width as the radionuclide image. Accurate spatial registration of the CT and radionuclide data is important since slight differences in position of the attenuation map relative to the corresponding data can cause ‘edge artefacts’ which produce bright and dark ‘rims’ across edges of regions where the CT and radionuclide data are misaligned.

The process of generating attenuation maps as described above also assumes that the body is composed primarily of lean soft tissue (essentially

water-equivalent) and bone. However, CT studies of the head and body generally are obtained following the administration of intravenous and oral contrast media.⁸⁶ Since contrast media in the body can attenuate photons emitted by a radiopharmaceutical during a PET or SPECT study, it obviously is important to derive accurate attenuation maps that account for the presence of these materials in the body regardless of whether they are administered orally and/or intravenously.^{42,69,86,87} It has been shown that SPECT and PET attenuation can be overestimated in the presence of positive contrast agents, which can generate significant artefacts (Figure 7). One can account for attenuation differences between iodine versus bone using a technique that generates a calibration curve for contrast media, using a method similar to that described above for soft tissue and bone alone. In this method, calibration data are obtained experimentally using CT to image a calibration phantom containing known concentrations of iodine contrast. The reconstructed CT values for each calibration region in the phantom are extracted from the CT scan, and are related to the known linear attenuation coefficients as a function

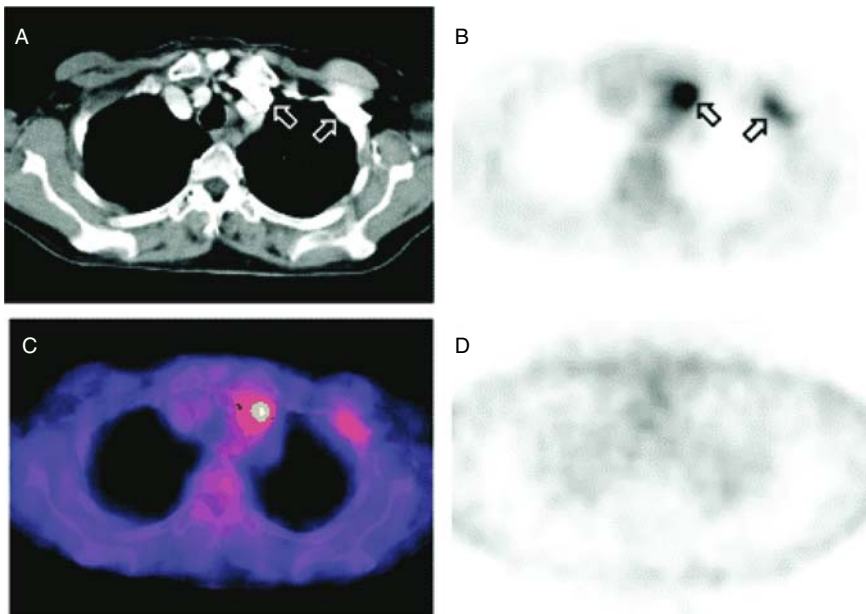


FIGURE 7. Contrast-enhanced related artefact in PET/CT imaging. Bolus passage of intravenous contrast agent in left subclavian and brachiocephalic veins on CT (A, arrows) led to areas of apparently increased glucose metabolism on CT-based attenuation corrected PET (B, arrows). On fused PET/CT images, this area of apparently increased glucose metabolism correlated with high-density contrast in venous system on CT (C). Reconstructed PET images without attenuation correction demonstrated homogeneous tracer distribution (D), demasking areas of apparently increased glucose metabolism as artefact. Reprinted with permission from ref.⁸⁶

of CT number. Separate calibration curves are generated for each material (i.e., iodine vs. bone), for different x-ray potentials used to acquire CT scans, and for different photon energies (e.g. 140 keV, 364 keV, and 511 keV) encountered in nuclear medicine.^{42,69} It is important to use image processing or other techniques to segment bony and iodine-containing regions in the patient's CT image so that bone and iodine can be scaled independently when forming the attenuation map. The attenuation maps with calibrated values for soft-tissue, fat, bone, and iodine, then are incorporated into an ML-EM or other iterative reconstruction algorithm for attenuation compensation of the radionuclide image. These methods have been tested in phantoms and in animals, and demonstrated in pilot studies on humans.

The x-ray data from a dual-modality imaging system also can be used to compensate the radionuclide data for contamination by scatter radiation (see chapter 7). One class of scatter compensation techniques characterizes the scatter distribution for different radionuclide and attenuation distributions with a spatially-dependent kernel, which can be used to convolve data from the photopeak window for estimating the scatter distribution from the acquired data. For example, the method proposed by Mukai *et al.*⁸⁸ assumes that the scatter radionuclide image ρ can be estimated from the "true" (i.e., "scatter-free") image η , as $\rho = P\eta$, where P is a matrix having elements $P(b, b')$ specifying the probability that a primary photon emitted from voxel b' is scattered in voxel b with an energy suitable for detection within the primary energy window and which can be calculated by integrating the Klein–Nishina equation over the primary acquisition energy window taking into account the energy resolution of the emission system. Obviously, the "true" or "scatter-free" image is unknown, making it necessary to approximate this using the currently available image estimated by the tomographic reconstruction algorithm. The matrix P can be approximated from the coregistered CT-derived attenuation map of the object provided by the dual-modality imaging system to obtain the total attenuation ($\Delta(b, b')$) along a line from the center of voxel b to the center of voxel b' . All the parameters needed can be determined accurately from x-ray based attenuation maps, illustrating how this process is facilitated by the availability of CT data from dual-modality imaging. Once the scatter distribution is calculated, it can be incorporated in the tomographic reconstruction algorithm to compensate the radionuclide data for the effect of this perturbation.

The visual quality and quantitative accuracy of the radionuclide data can be improved by using the methods described above by image fusion with CT, and use of x-ray data to correct the radionuclide data for perturbations arising from photon attenuation and Compton scatter. In addition, the radionuclide image can be improved by correcting the data for the geometric response of the radionuclide detector.^{6,42,89,90} Traditionally, radionuclide quantification methods have focused on techniques that compensate the radionuclide image reconstruction process for physical errors such as photon attenuation, scatter radiation, and partial volume errors as discussed above. This may include the

use of recovery coefficients,⁸⁹ requiring *a priori* information about object size and shape, that generally are only used for simple target geometries (e.g., spheres). Other investigators have developed methods that incorporate physical models, not in image reconstruction, but rather into the quantification process itself. Several methods have been described in the literature combining SPECT and MRI⁹¹ and PET and MRI^{92,93} for brain imaging, and SPECT and CT for cardiac and oncologic imaging.^{21,59,69} Several approaches were developed specifically for quantitation using planar imaging^{65,94,95} and are described in chapter 13 of this book. One technique called “template projection”^{42,90} can be used to quantify radioactivity in planar images. This process begins with dual-modality (i.e., radionuclide and CT) images of a target region surrounded by background. Regions-of-interest (ROIs) for the target (e.g., tumour) and background regions are defined on the high-resolution CT image, then are used to define “templates” which represent idealized radionuclide-containing objects (e.g., tumour vs. background) with unit radionuclide concentration. Planar imaging of these ideal radionuclide objects is modelled by mathematically projecting the templates onto the plane of the radionuclide detector using the known geometrical transformation between the CT coordinate system and the planar radionuclide image provided inherently by the dual-modality imaging system. This is performed using the projection machinery available from iterative reconstruction algorithms (e.g., ML-EM), including physical models of photon attenuation and non-ideal detector response, and which potentially can incorporate perturbations from detected scatter radiation, patient motion, and pharmaceutical kinetics. This process generates “projected templates” that are analogous to conventional ROIs, in that they delineate a target region over which events in the radionuclide image are integrated. Like conventional ROIs, the projected templates specify the geometry of the tumour and background regions on the projected planar radionuclide images; however the projected templates are defined on the high-resolution CT images rather than on the low-resolution radionuclide images. Furthermore, unlike traditional ROIs which are uniform, the projected templates are nonuniform and contain information about physical effects (photon attenuation, detector response, scatter radiation) included in the projector model.

Several methods using the projected templates can quantify activity in a planar radionuclide image. If we assume that the imaging process is linear, and consider the photons emitted from M different regions (e.g., tumours and background) where each region has a uniform activity concentration A_m , then the counts $p(d)$ measured in detector (i.e., pixel) d are estimated by $p^*(d)$ as

$$p^*(d) = \sum_{m=1}^M A_m \phi_m(d) \quad (1)$$

where $\phi_m(d)$ represents the value of the projected template at detector location d , which is physically equivalent to the relative number of photons

detected from radioactive region m in pixel location d . If we measure the value $p(d)$ from the planar emission data and given that we have calculated $\phi_m(d)$ from the template-projection technique, we can estimate the activity concentration A_m for region m (i.e., for the target lesion) by minimizing the weighted least squares difference

$$\chi^2 = \sum_{d=1}^D \left[\frac{p(d) - \sum_{m=1}^M A_m \phi_m(d)}{\sqrt{p(d)}} \right]^2 \quad (2)$$

where D is the number of detector elements (i.e., pixels) from which we estimate the activity concentrations (typically an area surrounding the target lesion). We note that a theoretical basis for this formulation has been described elegantly by Formiconi⁹⁶ and is similar to a method described by Liu.⁹⁷ An alternative formulation assuming Poisson statistics was suggested by Carson.⁹⁸ Specific details of the implementation described here can be found elsewhere.⁴²

The template projection technique described above for planar imaging can be extended to quantify target regions in tomographic images. This technique, called “template projection-reconstruction”,⁴² begins with the “template projection” technique described above. This process is repeated for all angles sampled by the tomographic acquisition of the real radionuclide data. After the template projection data for the target and for the background structures are modelled, they are reconstructed with the same reconstruction algorithms (e.g., ML-EM or filtered-backprojection) that are used for reconstructing the emission data. The reconstructed templates contain information about physical effects (e.g., photon attenuation, scatter radiation, geometric response) included in the modelling process and can be used to quantify the emission tomographic data. Several methods are then available for estimating the object activity concentration. For example, the radionuclide content of the target region can be calculated using a technique analogous to that discussed above for planar imaging by assuming that both the imaging and reconstruction processes are linear. With this assumption, the reconstructed activity concentration $\rho(i)$ of each voxel of the radionuclide image is represented as a linear combination of the M radionuclide concentrations A_m (assumed to be uniform) in the different regions, weighted by their corresponding reconstructed template values $\gamma_m(i)$

$$\rho(i) = \sum_{m=1}^M A_m \gamma_m(i) \quad (3)$$

where $\gamma_m(i)$ represents the contribution of activity region m to measured counts in reconstructed voxel i , as estimated from the template projection-reconstruction process. The activity concentrations of each object may be

obtained by linear least squares fitting analogous to that given by Eq. 2. Alternatively, the corrected mean activity concentration ρ_t in the target region can be calculated through voxel-by-voxel rescaling after estimating or assuming the background activity concentration ρ_b .

$$\rho_t = \frac{1}{N} \sum_{i=1}^N \frac{\rho(i) - \rho_b \gamma_b(i)}{\gamma_t(i)} \quad (4)$$

where $\gamma_b(i)$ and $\gamma_t(i)$ represent the reconstructed template values for voxel location i and contributed by the background (b) and target (t) regions, respectively. The voxel-by-voxel correction is analogous to scaling the reconstructed data with object size- and shape-dependent recovery factors^{42,89,99} (i.e., by division by $\gamma_t(i)$ and corrects for “spill-in” of background activity into the target lesion (by subtraction of the term $\rho_b \gamma_b(i)$). The radionuclide content of a given target region t , can be calculated as $\rho_t V_T$, where V_t is the actual target volume defined on the CT image.

At present, dual-modality imaging is most widely used to enable spatial registration of structural and functional information from CT and radionuclide imaging. Attenuation correction of radionuclide data using a CT-derived patient-specific map of attenuation coefficients also is available with all dual-modality imaging systems. However, very few clinical or biological studies have been conducted that use quantification methods such as template projection, template projection-reconstruction, or other model-based methods that extract *a priori* anatomical information for analysis of functional data from PET or SPECT. However, these techniques are being developed and are slowly being incorporated into research studies. For example, Koral *et al.*⁹⁹ have developed a technique that uses CT-SPECT image fusion with conjugate view imaging to quantify the uptake of single-photon radionuclides *in vivo*. In this analysis, a patient-specific attenuation map is derived from the correlated CT images to correct the radionuclide data for photon attenuation. In addition, volumes of interest delineating the extent of the tumour are defined anatomically on the CT scans, then are superposed on the SPECT data for radionuclide quantification^{100,101}. Excellent results have been obtained with this method to assess radiation dosimetry of lymphoma patients undergoing radionuclide therapy with ¹³¹I-tositumomab, also known as the anti-B1 monoclonal antibody.^{65,94} An initial study showed that the percentage of infused dose in the tumour following therapeutic administration of the agent could be predicted within 8% by linear extrapolation of the uptake of tracer amounts infused before therapy.⁹⁴ A later study demonstrated that the probability of complete response using radionuclide therapy was correctly associated with a high tumour dose measured in the patient using the SPECT-CT analysis.⁶⁵ Furthermore, for individual tumours, the combined SPECT-CT method provided a statistically significant relationship between radiation dose and tumour volume reduction at 12 weeks whereas this relationship was not

significant for dosimetry estimated from a conventional pre-therapy conjugate view radionuclide imaging alone.^{102,103} Koral *et al.* developed the quantification method using images obtained using separate SPECT and CT studies and that were combined using software-based image registration; however, the quantification technique certainly could be implemented using a dual-modality SPECT/CT system of the type described in this chapter. The reader is directed to a more extensive discussion of planar radionuclide quantification techniques in chapter 13. Radionuclide quantification also can be implemented using SPECT/CT, PET/CT, and other dual-modality imaging approaches of the type described in this chapter.¹⁰⁴

4. General Design Features of Dual-Modality Imaging Systems

Modern dual-modality imaging systems incorporate subsystems for radionuclide imaging and for x-ray computed tomography that essentially use the same components as those in dedicated nuclear medicine and CT systems. In PET/CT, the radionuclide detector uses a scintillator (bismuth germinate, lutetium orthosilicate, gadolinium orthosilicate) coupled to an array of photomultiplier tubes for imaging the annihilation photons from the positron-emitting radiopharmaceuticals. Modern PET/CT scanners also include an x-ray source and detector identical to those used in modern multislice helical scanning CT scanners.³³⁻³⁵ Similarly, SPECT/CT systems use conventional dual-headed scintillation cameras suitable for planar scintigraphy or tomographic imaging of single-photon radionuclides, or coincidence-imaging of PET radiopharmaceuticals. The first-generation clinical SPECT/CT scanners used a low-resolution CT detector^{40,41,70,105} that offered relatively modest scan times (i.e., approximately 20 seconds per slice). However, newer SPECT/CT scanners now are becoming available that incorporate state-of-the-art multislice helical CT scanners identical to those used for diagnostic CT procedures.

The integration of the radionuclide and x-ray imaging chains in a dual-modality imaging system requires special considerations beyond those needed for scanners designed for single modality imaging alone. One challenge is offered by the presence of x-ray scatter from the patient that has the potential to reach and possibly damage the radionuclide detectors which are designed for the relatively low photon fluence rate encountered in radionuclide imaging.^{34,35,64} To avoid this possibility, the radionuclide detector in a dual-modality system typically is offset in the axial direction from the plane of the x-ray source and detector. This distance can be relatively small when a modest x-ray tube is used such as the 140 kV, 1 mA tube used in the GE Millennium VG SPECT/CT system,⁶⁴ but can be 60 cm or more when a

diagnostic CT scanner is coupled to a modern PET scanner operated without septa.^{28,30,31,34}

As noted above, all dual-modality systems rely on separate x-ray and radionuclide imaging chains that must be supported on a common mechanical gantry to maintain consistent spatial relationship between the two data sets, and allow the detectors to be rotated and positioned accurately for tomographic imaging. The requirements for translational and angular positioning accuracy are, of course, different for CT, SPECT, and PET. For example, CT requires approximately 1000 angular samples acquired with an angular position and center of rotation maintained with submillimeter accuracy. In comparison, SPECT and PET have spatial resolutions of a few millimetres, and therefore can be performed with an accuracy of slightly less than a millimetre for clinical imaging.

The mechanical gantry of the dual-modality imaging system obviously must be designed to satisfy the requirements for both the radionuclide image and for CT. This can be achieved in several ways. In first generation SPECT/CT systems,^{40,41,70,105} the SPECT detectors and CT imaging chain were mounted on the same rotating platform and were used sequentially while rotated around the patient. This limited the rotational speed of the x-ray and radionuclide imaging chains to approximately 20 sec per rotation, but also had the advantage that it could be performed using a gantry similar to that used with a conventional scintillation camera. Second generation SPECT/CT systems that now are available include high-performance diagnostic CT subsystems. This requires the heavy SPECT detectors to be mounted on a separate rotating platform from the CT imaging chain which is rotated at speeds of 0.25 to 0.4 sec per revolution. While this design obviously increases the performance of the CT subsystem, it also increases the cost and complexity of the gantry.

In comparison to SPECT/CT in which the radionuclide detector is rotated around the patient during data acquisition, PET typically (but not always) is performed using a dedicated high-end stationary detector ring. A PET/CT system therefore can be configured by designing a gantry that mounts a stationary PET detector ring in tandem with a platform that rotates the CT imaging chain around the patient using a mechanical configuration similar to that used in a conventional diagnostic CT scanner. Alternatively, a partial ring of PET detectors can be rotated to acquire the PET data using the same rotating platform as the CT subsystem. This approach was taken by Townsend and his colleagues in their implementation of the first PET/CT system,^{28,30,31} and is an alternative for a more economical dual-modality system in comparison to those that use a full-ring of PET detectors. All of these mechanical designs have been used in commercial dual-modality systems and obviously offer trade-offs in terms of their performance and cost.

The patient table is another seemingly simple, yet important element of a dual-modality scanner.^{34,35} Most imaging systems use cantilevered patient tables to support the patient in the bore of the imaging system. Patient tables

are designed to support patients weighing up to 500 pounds, but obviously deflect to varying degrees when they are loaded and extended with normal adult patients. However, dual-modality systems use x-ray and radionuclide imaging chains in tandem and thereby require longer patient tables than conventional imaging systems. Moreover, the table extension and the degree of deflection can be different for the x-ray and radionuclide imaging chains which can introduce a patient-dependent inaccuracy in the registration of the x-ray and radionuclide images. This problem is overcome by several different methods. The first uses a patient table which is supported in front of the scanner, with a secondary support between or at the far end of the x-ray and radionuclide imaging chains to minimize table deflection. A second approach adopted by CTI Molecular Imaging and Siemens Medical Systems uses a patient table that can be fixed on a base that is translated across the floor to extend the patient into the scanner. Since the patient platform is stationary relative to its support structure (which acts as a fulcrum), the deflection of the patient table is identical when the patient is positioned in the radionuclide imager or the CT scanner.

Finally, in modern dual-modality scanners, the computer systems are well integrated in terms of system control, data acquisition, image reconstruction, image display, and data processing and analysis.^{34,106} The dual-modality system must calibrate the CT data so that it can be used as an attenuation map to correct the radionuclide data for photon attenuation.^{21,22,27,29,42,44} For physician review, the dual-modality system also typically registers the CT and radionuclide data and presents the radionuclide image as a colour overlay on the grey-scale CT image. Finally, software tools are provided that, for example, allow a cursor placed on the CT image by the operator with another cursor automatically placed in the identical position on the radionuclide image, and vice versa. These software functions allow the operator to utilize the dual-modality data in correcting, viewing, and interpreting and obviously are important design elements in modern dual-modality imaging systems.

5. PET/CT Imaging Systems

The first combined PET/CT system was developed by Townsend and co-workers at the University of Pittsburgh in 1998.^{28,33,34} The system was configured by combining a Somatom AR.SP spiral CT scanner (Siemens Medical Systems) in tandem with the PET detectors from an ECAT ART PET system (CTI/Siemens). The PET subsystem consisted of two arrays of bismuth germanate (BGO) block detectors covering 16.2 cm in the axial direction with 24 partial detector rings operated without septa, allowing the PET data to be acquired in a fully 3-dimensional mode. The CT scanner was a third generation helical CT scanner that has an x-ray tube operated at 110-130 kVp with a 6.5 mm Al-equivalent filtration and having a xenon

x-ray detector with 512 elements. Both the CT components and the PET detectors are mounted on opposite surfaces of the rotating stage of the CT system, and during imaging are rotated continuously at a rate of 30 rpm. The system has a common patient table, with the patient translated between the centers of the CT and PET imaging planes which were offset axially by 60 cm. On the prototype system, an axial extent of 100 cm in the patient could be covered by simple table translation^{33,34} with the PET and CT images acquired sequentially rather than simultaneously. The PET/CT prototype was operational at the University of Pittsburgh from May 1998 to August 2001, during which over 300 cancer patients were scanned. These pioneering studies by Townsend and his colleagues demonstrated both the feasibility and the clinical benefit of combined PET/CT scanning, and prompted significant interest from the major medical imaging equipment manufacturers who now all have introduced commercial PET/CT scanners for clinical use.

PET/CT scanners now are available from all of the major medical imaging equipment manufacturers (GE Medical Systems, CTI/Siemens Medical Systems, and Philips Medical Systems).^{35,107} Current systems have up to 16 slice CT capability and have radionuclide detectors with either 2D or 3D PET imaging capability. The PET scanner can have either bismuth germinate (BGO), lutetium oxyorthosilicate (LSO), or gadolinium oxyorthosilicate (GSO) scintillators. The CT study typically is used for both localization of the FDG uptake^{38,41,61} as well as for attenuation correction of the PET image. In addition, the use of CT in comparison to external transmission rod sources for producing the attenuation data increases patient throughput by approximately 30%.¹⁰⁷ As noted above, the PET/CT system also has a specially designed patient table that is designed to minimize deflection when it is extended into the patient port.

Figure 8 shows the 7 steps identified by Beyer *et al.*¹⁰⁸ that comprise a typical PET/CT scan, demonstrating the degree of integration available in a modern dual-modality imaging system. (1) The patient is prepared for imaging which commonly includes administration both with contrast media⁸⁶ and with the radiopharmaceutical, typically 370 to 555 MBq (10 to 15 mCi) of ¹⁸F-fluorodeoxyglucose (FDG) in adults. (2) The patient then is asked to remove all metal objects that could introduce artefacts in the CT scan and then is positioned on the patient table of the dual/modality imaging system. (3) The patient then undergoes an “overview” or “scout” scan during which x-ray projection data are obtained from the patient to identify the axial extent of the CT and radionuclide study. (4) The patient undergoes a CT acquisition. (5) The patient then undergoes the nuclear medicine study approximately 1 hour after FDG administration. (6) The CT and PET data then are reconstructed and registered, with the CT data used for attenuation correction of the reconstructed radionuclide tomograms. (7) The images are reviewed by a physician who can view the CT scan, the radionuclide images, and the fused x-ray/radionuclide data, followed by preparation of the associated clinical report.

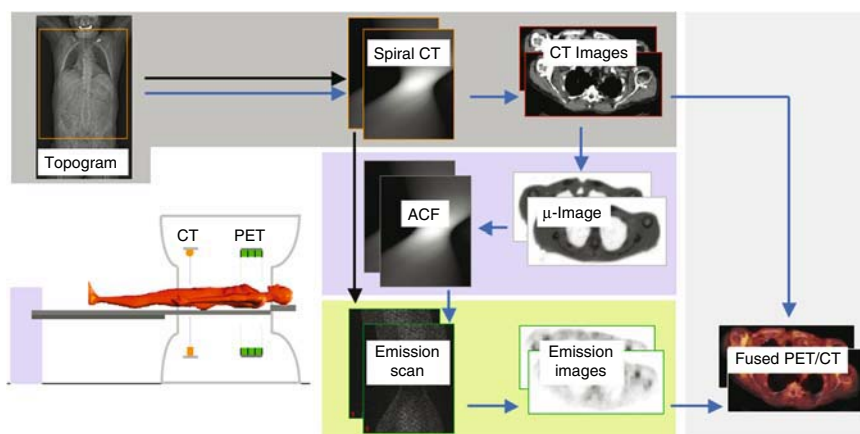


FIGURE 8. Illustration of standard PET/CT scanning protocol. The patient is positioned on a common specially designed patient table in front of the combined mechanical gantry. First, a topogram is used to define the co-axial imaging range (orange). The spiral CT scan (grey box) preceded the PET scan (green box). The CT data are reconstructed on-line and used for the purpose of attenuation correction of the corresponding emission data (blue box). Black and blue arrows indicate acquisition and data processing streams, respectively. Reprinted with permission from ref.¹⁰⁸

There have been multiple studies which have demonstrated the role of PET/CT especially for oncologic applications.¹¹⁰ For example, in a clinical study of PET/CT for the evaluation of cancer in 204 patients with 586 suspicious lesions, PET/CT provided additional information over separate interpretation of PET and CT in 99 patients (49%) with 178 sites (30%).¹⁰⁹ Furthermore, PET/CT improved characterization of equivocal lesions as definitely benign in 10% of sites and as definitely malignant in 5% of sites. It precisely defined the anatomical location of malignant FDG uptake in 6%, and led to the retrospective lesion detection on PET or CT in 8%. As a result, PET/CT had an impact on the management of 28 patients (14%), obviated the need for further evaluation in 5 patients, guided further diagnostic procedures in 7 patients, and assisted in planning therapy in 16 patients. Figure 9 shows an example of a patient study where the combined PET/CT images provided additional information, thus impacting the characterization of abnormal FDG uptake.

6. SPECT/CT Imaging Systems

As noted earlier, the first SPECT/CT imaging systems were developed at the University of California, San Francisco by Hasegawa and co-workers. The first prototype instruments (Figures 2 and 3) were configured as small-bore

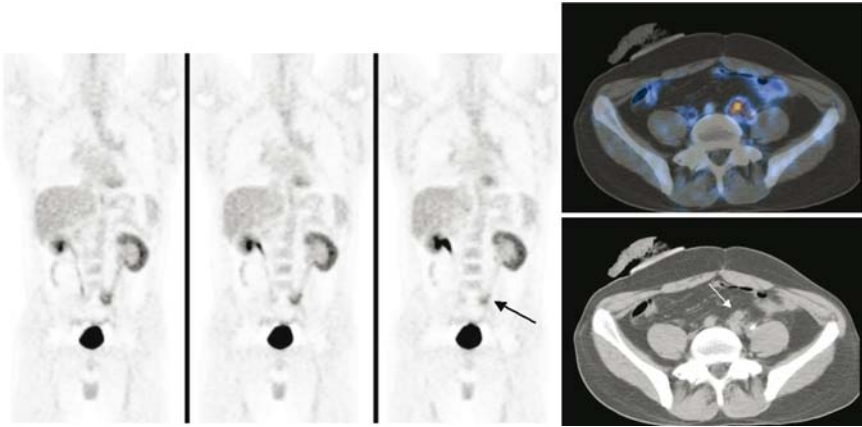


FIGURE 9. Precise characterization of increased ^{18}F -FDG uptake and retrospective lesion detection on CT, after PET/CT. The patient is a 35-y-old man, 22 months after treatment of colon cancer, with negative high-resolution contrast-enhanced CT and normal levels of serum tumour markers, referred for PET scan for assessment of pelvic pain. The coronal PET images (left) show area of increased ^{18}F -FDG uptake in left pelvic region (arrow), interpreted as equivocal for malignancy, possibly related to inflammatory changes associated with ureteral stent or to physiological bowel uptake. Hybrid PET/CT (right) transaxial image (top) precisely localized uptake to soft-tissue mass adjacent to left ureter, anterior to left iliac vessels. Mass (arrow) was detected only retrospectively on both diagnostic CT and CT component of hybrid imaging study (bottom). Patient received chemotherapy, resulting in pain relief and decrease in size of pelvic mass on follow-up CT. Reprinted with permission from ref.¹⁰⁹

SPECT/CT systems with a small segmented high-purity germanium detector operated in pulse-counting mode for simultaneous x-ray and radionuclide imaging.^{23,26,57,59} A clinical prototype SPECT/CT system (Figure 4) also was configured at UCSF by installing a GE X/RT SPECT camera and GE 9800 CT scanner in tandem with a common patient table,^{21,22,42,69} and was used for studies on both large animals and patients.

The first dual-modality imaging system designed for routine clinical use was the Millennium VG (Figure 10) introduced by General Electric Healthcare Technologies (Waukesha, WI) in 1999.^{40,41,70,105} This system has both x-ray and radionuclide imaging chains that were integrated on a common gantry for “functional-anatomical mapping”. X-ray projection data are acquired by rotating the x-ray detector and low-power x-ray tube 220 degrees around the patient. Since the patient is not removed from the patient table, the x-ray and radionuclide images are acquired with a consistent patient position in a way that facilitates accurate image registration. The image acquisition of the CT data requires approximately five minutes, and the radionuclide data requires a scan time of approximately 30 to 60



FIGURE 10. GE Millennium VG SPECT system with x-ray anatomical mapping. Reprinted with permission from General Electric Healthcare Technologies, Waukeasha, Wisconsin.

minutes. These SPECT/CT systems produce transmission data with significantly higher quality and better spatial resolution than those acquired with an external radionuclide source, and can be used for anatomical localization¹⁴ and attenuation correction of the radionuclide data.

In June 2004, both Siemens Medical Systems and Philips Medical Systems introduced SPECT/CT systems offering the performance available on state-of-the-art diagnostic CT systems. For example, Siemens Medical Systems now offer their Symbia line of SPECT/CT systems that have a single-slice, 2-slice, or 6-slice CT options with 0.6 sec rotation speed coupled to a dual-headed variable-angle SPECT system. The 6-slice CT scanner will cover the abdomen in less than 6 seconds and allows both x-ray based attenuation correction and anatomical localization with the correlated diagnostic CT images. Philips Medical Systems has announced their Precedence SPECT/CT system which incorporates a dual-headed SPECT system with a 16 slice diagnostic CT scanner. The advanced CT capability has several potential benefits. First, they offer CT scan times that are compatible with the use of contrast media for improved lesion delineation with CT. Second, they offer improved image quality and spatial resolution typical of that offered by state-of-the-art diagnostic CT scanners. Finally, CT scanners offering 16 or more slices can be used for cardiac and coronary imaging. SPECT/CT scanners with multislice capabilities therefore offer improved performance for tumour imaging and have the potential to acquire and overlay radionuclide myocardial perfusion scans on a CT coronary angiogram showing the underlying arterial and cardiac anatomy in high spatial resolution.

7. Small-Animal Imaging Systems

The advantages of improved image quality and quantitative accuracy that are available for clinical applications of dual-modality imaging also are being investigated as a means of facilitating biological research, especially those that involve small animals such as mice and rats.^{37,111} Advances in molecular biology and genetic engineering, and the modern growth of the pharmaceutical and biotechnology industries have increased the need for biological studies that involve mice. Approximately 90% of all research involving vertebrate biology now uses mice as the predominant mammalian model.¹¹² Approximately 25 million mice were raised in 2001 for experimental studies, and this number is expected to increase at a rate of 10% to 20% annually over the next decade. In addition, experimental methods now allow the genetic sequence of mice to be manipulated by knockout or transgenic techniques in which a genetic sequence from another individual or species can be deleted or inserted into that of an individual animal. Murine models now are available for a wide variety of biological conditions and transgenic animals¹¹³⁻¹¹⁶ now account for a sizable and growing fraction of animal models used in biological research.

Traditional techniques of biological research including histology, organ sampling, and autoradiography, require that animals must be sacrificed for the measurement to be obtained. This precludes investigators from obtaining multiple measurements from an individual during the progression of disease or while an animal is monitored following diagnostic procedures or therapeutic interventions. This greatly increases the number of animals that must be used for an individual experiment, compromises statistical power, and requires that control and experimental measurements are made in different rather than in the same animal.

While noninvasive imaging techniques potentially could be used in these experiments to obtain the desired measurements, clinical medical systems do not have adequate spatial resolution and temporal resolution, and other specific characteristics needed to image small animals. For example, for cardiovascular studies, the left heart of a mouse in short axis view is approximately 5 mm in diameter with the left ventricular wall having a thickness of approximately 1 mm. In addition, the mouse heart rate is 600 to 900 beats per minute making it difficult to acquire image data with cardiac gating.^{116,117} Similarly, small tumours can have a diameter of a few millimetres, within the spatial resolution limit of clinical CT and MRI systems but outside that of conventional radionuclide imaging such as SPECT or PET. For these reasons, investigators have developed high resolution imaging systems specifically designed for small animal imaging.^{111,112,118-120} These include microCT systems^{118,121-123} that incorporate a low power X-ray tube and a phosphor-coupled CCD camera or similar two-dimensional x-ray imaging detector to achieve spatial resolutions as high as 25 microns or

better. Similarly, high-resolution images can be obtained using microPET scanners^{111,119} having high-resolution detectors operated in coincidence to obtain spatial resolutions in the range of 1 to 2 mm, whereas SPECT imaging of mice¹²⁴⁻¹²⁹ can be performed using pinhole collimation to obtain spatial resolutions better than 1 millimetre. In general, these imaging systems provide characteristics similar to those used for clinical imaging of humans. In the specific case of radionuclide imaging, including microPET and micro-SPECT, the accumulation of radiotracer can be used to monitor physiological or biological interactions in the animal. Dual-modality imaging offers potential advantages in biological studies, similar to those offered in clinical protocols.^{120,130-138} First, the availability of anatomical data improves localization and interpretation of studies involving radiopharmaceutical uptake. In addition, the visual quality and quantitative accuracy of small animal imaging can be improved using x-ray based techniques to correct the radionuclide data for physical errors contributed by photon attenuation, scatter radiation, and partial volume effects due to the limited spatial resolution of the radionuclide imaging system.

In response to these concerns, several investigators now are developing dual-modality imaging systems specifically designed for imaging small animals.³⁷ Dr. Cherry and his group, now at the University of California at Davis, have developed a microPET system for small-animal imaging. Commercial versions of these microPET systems suitable for imaging mice and rats now are available from CTI Concorde Microsystems (Knoxville, TN). The same group also has developed a microCT/microPET dual-modality imaging system.¹³¹ The microPET detectors use LSO scintillator coupled through a fiber-optic taper to a position sensitive photomultiplier tube. These are placed on opposite sides of the animal with the annihilation photons from the positron emission detected in coincidence. The system also includes a microCT system having a microfocus x-ray tube and an amorphous selenium detector coupled to a flat panel thin film resistors readout array.¹³⁹ A schematic diagram of a prototype system and an image of a mouse obtained with the microPET/microCT system are shown in Figure 11.

SPECT/CT systems designed specifically for small animal imaging also are being developed by several investigators.^{120,132-138,140,141} One of the first small animal SPECT/CT systems was developed by a consortium that includes The Thomas Jefferson National Accelerator Facility (Jefferson Laboratory), The University of Virginia, and researchers at the College of William and Mary.¹³²⁻¹³⁴ These systems use a compact scintillation camera that operates with multiple Hamamatsu R3292 position-sensitive photomultiplier tubes (PSPMT's) coupled to a pixelated array of cesium iodide (CsI(Tl)) crystals using both pinhole and parallel-hole collimators. The x-ray data are acquired using a small fluoroscopic x-ray system (Lixi, Inc., Downers Grove, IL). Representative planar dual-modality images acquired on one of the systems mentioned above obtained from a 250-g rat injected with

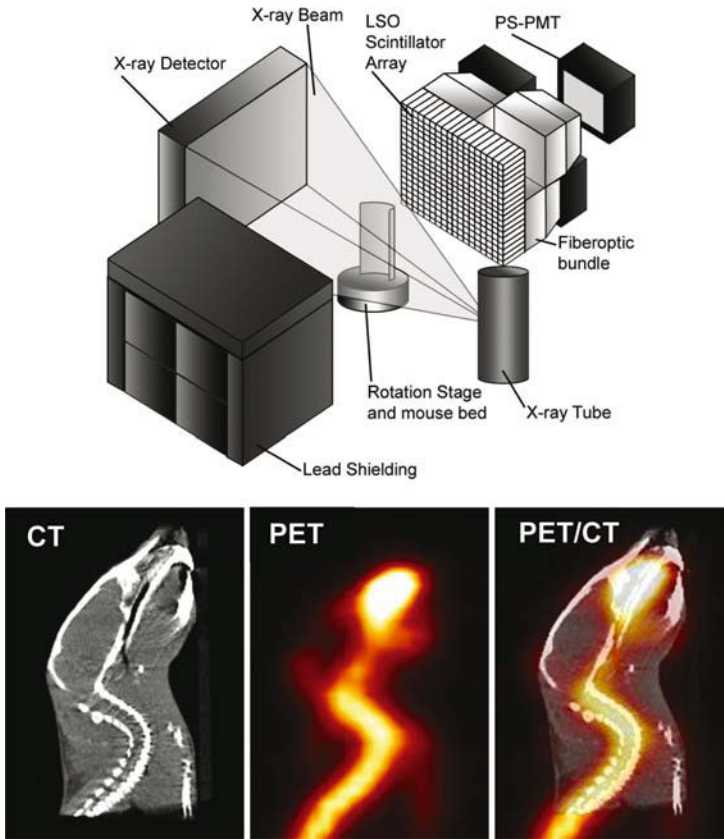


FIGURE 11. Top: schematic diagram of the experimental set-up. The CT and PET components are mounted in a coplanar geometry so that the same portion of the mouse is imaged by both systems at once. The back PET detector is shown without the lead shielding in place in order to show the design of the detector modules. The lead shielding on the entrance face is 1.5 mm thick. The detectors remain stationary while the object is rotated on the bed mounted on the rotation stage. Bottom: scan of a mouse 3 hours after injection of 26 MBq of ^{18}F bone seeking tracer. The images shown are from left to right: sagittal slices through the CT image, the ^{18}F PET image, and the fused PET/CT image. Note the overlap of the PET uptake with the location of the bones in the CT image. The scan was acquired using 400 views in a time of 38 min. Reprinted with permission from ref.¹³¹

$^{99\text{m}}\text{Tc}$ -MDP are shown in Figure 12, demonstrating radiopharmaceutical uptake in the bone superimposed with an anatomical x-ray image of the rat.^{133,142}

Gamma Medica[™] Inc. (Northridge, CA) has developed and introduced a small animal SPECT/CT system^{137,138} with two compact scintillation cameras^{126,143,144} and a high-resolution CT subsystem¹³⁸ for dual-modality

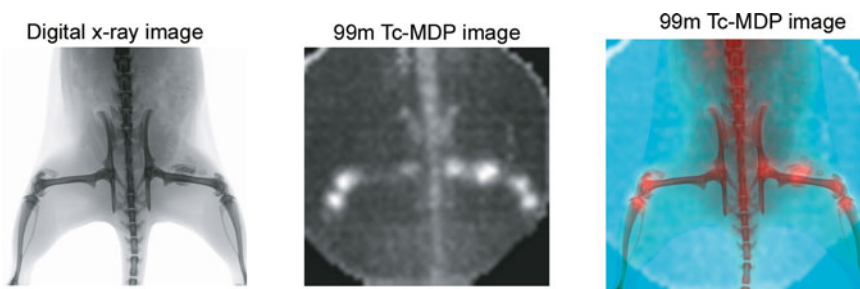


FIGURE 12. Superposition of digital x-ray radiography (left) and radionuclide $^{99\text{m}}\text{Tc}$ -MDP bone scan (middle) resulting in a fused image of the rear portion of a rat (right). (Courtesy of Dr Mark B. Williams, University of Virginia).

imaging of mice, rats, and other small animals (Figure 13). The scintillation camera can be operated with pinhole collimators that provide submillimeter spatial resolution in the reconstructed images or with parallel-hole collimators when higher detection sensitivity or whole body imaging is desired. The system includes a high-resolution microCT subsystem¹³⁸ configured with a CMOS x-ray detector coupled to a gadolinium oxysulfide scintillator and a low-power x-ray tube. The microCT system provides anatomical imaging with a spatial resolution of approximately 50 microns; the resulting x-ray data can be used both for attenuation correction and for anatomical localization of the radionuclide data (Figure 14). In addition, the radionuclide data can be acquired with ECG-gating for cardiovascular imaging applications where wall-motion abnormalities, ejection fraction calculations, or other assessments of ventricular function are necessary.



FIGURE 13. Gamma Medica X-SPECT system has dual-headed compact SPECT system and high-resolution microCT imaging capability. Reprinted with permission from Gamma Medica, Incorporated, Northridge, CA.

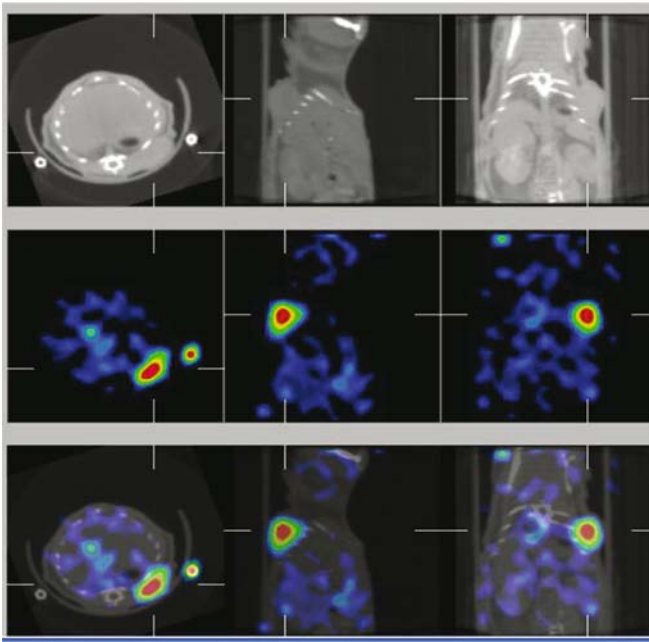


FIGURE 14. X-ray CT (top row), SPECT (middle row), and coregistered SPECT/CT (bottom row) obtained with small animal dual-modality system (X-SPECT, Gamma Medica, Northridge, CA) of colon carcinoma xenograft in right shoulder of mouse. SPECT images recorded 23 hours after administration of ^{123}I -labeled anti-CEA minibody¹⁴⁵ that localizes in colon carcinoma. Images shown in transverse (left column), sagittal (middle column), and coronal (right column) tomograms. (Images from G Sundaresan, S Gambhir, AM Wu, with permission from AM Wu, UCLA, Los Angeles, CA, and reprinted with permission from ref.¹⁴⁶

Finally, the Center for Gamma Ray Imaging at the University of Arizona, under the direction of Dr Barrett, has configured a high-resolution SPECT/CT system for small animal imaging.¹³⁵ High-resolution SPECT is performed with a modular semiconductor detector that consists of a $2.5 \times 2.5 \times 0.2 \text{ cm}^3$ slab of cadmium zinc telluride (CdZnTe) operated with a continuous gold electrode to apply bias on one side, and a 64×64 array of pixelated gold electrodes on the opposite side connected to an ASIC for readout of the individual pixel signals. The detector has a $380 \mu\text{m}$ pixel pitch, and $330 \mu\text{m}$ wide pixels, coupled to a 7 mm thick parallel-hole collimator for radionuclide imaging. The x-ray and radionuclide imaging subsystems are mounted with their image axes perpendicular to one another with the animal rotated vertically within the common field of view. The x-ray and radionuclide projection data are acquired sequentially, and corrected for distortions

and nonuniformities introduced by each of the detectors, then reconstructed with statistical iterative algorithms (OS-EM).

8. Need for Dual-Modality Imaging

Even though both PET/CT and SPECT/CT systems have been accepted commercially, the clinical role and need of these systems is still being debated. PET, for example, is a diagnostic technique that offers a sensitivity and specificity in excess of 90% for many malignant diseases, and some argue that an incremental improvement in specificity or sensitivity beyond that point probably cannot justify the cost of performing image fusion for all patients on a routine basis.¹⁴⁷ Furthermore, a patient receiving medical diagnosis typically undergoes both anatomical and functional imaging from commonly-available single-modality medical imaging systems. This means that the anatomical images can be viewed side-by-side with the functional images when necessary. In other cases, image registration techniques^{15,16} can be used when a more direct fusion of anatomical and functional data following their acquisition without the use of the expensive new dual-modality imaging systems (see chapter 9).

Nonetheless, other practitioners now see important roles for dual-modality imaging in the sense that it offers important features for diagnostic studies and patient management.^{37,73,109} First, the anatomical and functional information from dual-modality imaging are supplementary and not redundant. As noted earlier, anatomical imaging is performed with techniques such as CT or MRI that have excellent spatial resolution and signal-to-noise characteristics, but that may offer relatively low specificity for differentiating disease from normal structures. In contrast, radionuclide imaging generally targets a specific functional or metabolic signature in a way that can be highly specific, but generally lacks spatial resolution and anatomical cues which often are needed to localize or stage the disease, or for planning therapy.^{36,39,41,148} Similarly, the availability of correlated functional and anatomical images improves the detection of disease by highlighting areas of increased radiopharmaceutical uptake on the anatomical CT or MRI scan, whereas regions that look abnormal in the anatomical image can draw attention to a potential area of disease where radiopharmaceutical uptake may be low. The information from CT supplements that from radionuclide imaging, and *vice versa*; therefore it generally is advantageous to view the CT and radionuclide images side-by-side during the diagnostic interpretation. In other cases, it can be valuable to view a fused dual-modality image in which the radionuclide data are presented as a colour overlay on the grey-scale CT image. The availability of a dual-modality imaging system facilitates this process in acquiring the functional and anatomical data with the patient in a consistent configuration and during a single study, in a way that is faster and more cost-efficient than attempting

to register the images by software after they are acquired on separate imaging systems. The dual-modality image data can be used to guide radiation treatment planning for example by providing anatomical and functional data that are important for defining the target volume as well as indicating normal regions that should avoid irradiation. Similar roles are played when the dual-modality data is used to guide surgical approach, biopsy, or other interventional procedures.⁷³

In addition, the anatomical and functional information from a dual-modality imaging system are complementary in that together they provide information that cannot be easily discerned from one type of image alone. This is best illustrated in oncologic applications where anatomical imaging often is needed to differentiate whether the radiopharmaceutical has localized in response to disease (e.g. in the primary tumour, lymphatic system, or metastatic site)^{38,39,41,68,73} or as part of a benign process (e.g. in the GI tract, urinary system, or in response to inflammation).³⁵ Moreover, the process of differentiating normal from abnormal uptake of ^{18}F -FDG can be complicated by the relative paucity of anatomical cues in the ^{18}F -FDG scan, making it necessary for the diagnostician to refer to anatomical images obtained from CT or MRI to correlate the structural and functional information needed to complete the analysis.

The potential advantages of dual-modality imaging are further illustrated by a meta-study of PET-CT fusion for radiotherapy treatment planning in non-small cell lung carcinoma (NSCLC). Paulino *et al.*¹⁴⁸ found that the use of FDG imaging with PET/CT may alter target volumes for radiation therapy treatment planning in 26 to 100% of patients with NSCLC compared with CT-based treatment planning alone. Approximately 15 to 64% had an increase in the planning target volume (PTV), whereas 21 to 36% had a decrease in PTV. Similarly, in a study at Duke University,¹⁴⁹ SPECT-CT was useful in detecting the 48% of patients with hypoperfused regions of the lung, and in 11% of patients this information was used to alter the radiation therapy fields to avoid highly functional lung tissue. In addition, PET/CT and SPECT/CT may have an important role in guiding radiation treatment planning in cancers of the brain, head and neck, cervix, and other areas including lymphoma and melanoma.¹⁴⁸ These examples are not exhaustive, but indicate the potentially important role of dual-modality imaging in guiding radiation treatment planning in comparison to techniques that use anatomical imaging with CT alone.

The complementary nature of dual-modality imaging also is demonstrated by the use of a CT-derived attenuation map and other *a priori* patient-specific information from CT that can be used to improve both the visual quality and the quantitative accuracy of the correlated radionuclide imaging. This occurs in myocardial perfusion imaging of $^{99\text{m}}\text{Tc}$ -sestamibi or thallium-201 where SPECT/CT can provide an attenuation map to compensate the radionuclide image for soft-tissue attenuation associated with false-positive errors. In both PET/CT and SPECT/CT, the use of CT-derived attenuation

map is also practical and cost-efficient in that with modern CT scanners it is generated in a few seconds, resulting in more efficient use of time than SPECT or PET scanners that use external radionuclide sources to record the transmission image. The resulting CT-derived attenuation map also is of significantly higher quality, and arguably is more accurate, than those acquired using scanning line sources available in conventional radionuclide imaging systems. As dual-modality imaging systems become available with faster and higher spatial-resolution CT systems, it may be possible to perform CT angiography of peripheral or coronary vessels that can be superimposed on a colour map of tissue perfusion or metabolism obtained with SPECT or PET.

9. Challenges of Dual-Modality Imaging

There are several challenges that face the use of dual-modality imaging, and that may represent inherent limitations in this technique. All currently-used dual-modality imaging systems record the emission and transmission data using separate detectors rather than a single detector. In addition, the x-ray and radionuclide imaging chains are separated by several tens of centimetres, to facilitate mechanical clearance and to avoid contamination of the radionuclide data by scatter radiation produced by the x-ray scan. One potential problem occurs when the patient moves either voluntarily or involuntarily between or during the anatomical and functional image acquisitions. This can occur, for example, when the patient adjusts his or her position while lying on the patient bed. Patient motion also occurs due to respiration, cardiac motion, peristalsis, and bladder filling, all of which can lead to motion blurring or misregistration errors between the radionuclide and CT image acquisitions.¹¹⁰ Traditionally, CT data were acquired following a breath-hold, whereas PET data were acquired over several minutes with the patient breathing quietly. However, these breathing protocols can lead to misregistration artefacts due to anatomical displacements of the diaphragm and chest wall during a PET/CT or SPECT/CT scan. For example, if the position of the diaphragm is displaced in the CT scan, which then is used as an attenuation map for the radionuclide data, this displacement can lead to an underestimate or overestimate of radionuclide uptake in the reconstructed emission data.⁶³ The discrepancy in diaphragmatic position between PET and CT can result in the appearance of the so-called “cold” artefact at the lung base (Figure 15). A recent study¹⁵⁰ noted that in 300 patients with proven liver lesions; approximately 2% appeared to have the lesion localized in the lung due to respiratory motion. Care therefore must be taken when interpreting results from patients with disease in periphery of the lung where noticeable radiopharmaceutical uptake may be contributed by respiratory-induced motion artefacts rather than disease.

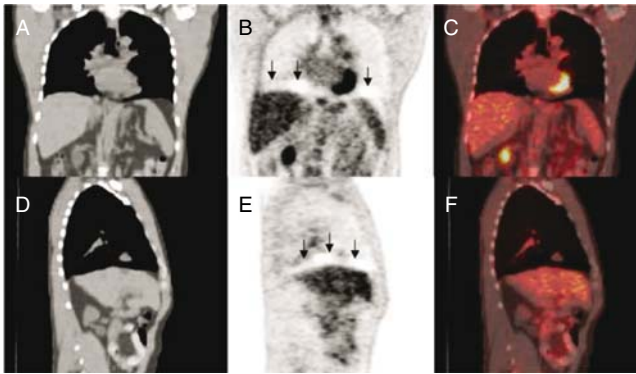


FIGURE 15. Demonstration of a cold artefact on PET images reconstructed with CT-based attenuation correction. (A) Coronal CT, (B) ^{18}F -FDG PET, and (C) fused, and (D) sagittal CT, (E) PET, and (F) fused images are displayed. A region of decreased metabolic activity is demonstrated in the diaphragmatic region (below vertical arrows), representing a “cold artefact”. Reprinted with permission from ref.¹¹⁰

Modern dual-modality scanners now use CT technology that can acquire the anatomical data within a few seconds after the patient is positioned on the bed. For this reason, the CT acquisition rarely is the factor that limits the speed of the dual-modality image acquisition in comparison to SPECT or PET that can consume several minutes to complete. If additional increases in scan speed are needed, these must be implemented using faster radionuclide scans using newer detector technologies, faster scintillators, increased computing power, and more efficient scanner architectures or detector designs than are currently being used. In PET, this includes the possibility of replacing conventional PET block detectors with LSO panel detectors^{35,151} which would cover a larger axial extent of the patient with the goal of achieving 5 min scan times and thereby would allow even faster scan times than are achievable with current systems. Regardless, faster scan speeds both improve patient comfort and limit the time during which patient motion can occur during the study. In addition, faster scan speeds can promote faster patient throughput and thereby increase system utilization and cost-effectiveness of the study.

Dual-modality imaging systems now commonly use the correlated CT scan as an attenuation map for the correction of the emission data acquired with PET or SPECT. The use of iodinated contrast media for the CT scan also presents a potential challenge when the CT scan is used as an attenuation map for correction of SPECT or CT data.⁸⁶ Since the x-ray energy of the CT data generally will be different than the photon energy of the radiopharmaceutical emission data, as described above, the CT data must be transformed to units of linear attenuation coefficient at the photon energy of the radiopharmaceutical emission data. This is performed by assuming

that image contrast in the CT data is contributed by mixtures of air, soft tissue, and bone. The presence of iodinated contrast complicates this process since two regions that have the same image contrast may indeed have different compositions, for example contributed by bone and soft tissue in one case and iodine contrast and soft-tissue in another situation. These artefacts are most severe in cases where the contrast media is concentrated, for example in abdominal imaging after the patient swallows a bolus of oral contrast. In this case, the higher densities contributed by the oral contrast media can lead to an overestimation of PET activity.⁸⁶ Some investigators have proposed using an image segmentation post-processing technique in which image regions corresponding to iodinated contrast are segmented using image processing from those contributed by bone.⁸⁷ In addition, other strategies including the acquisition of both pre-contrast and post-contrast CT scans, can be used to minimize possible artefacts contributed by the presence of contrast media when the CT scan is to be used as an attenuation map for correction of the PET data.³⁵

Use of dual-modality has demanded that technologists be cross-trained in both modalities, and that medical specialists have expertise in interpreting both anatomical and functional image data. Also, optimal use of SPECT/CT and PET/CT requires a team approach involving physicians from radiology and nuclear medicine, as well as oncology, surgery, and other clinical disciplines.

10. Future of Dual-Modality Imaging

Over the past 10 to 15 years, dual-modality imaging has progressed steadily from experimental studies of technical feasibility to the development of clinical prototypes to its present role as a diagnostic tool that is experiencing widening commercial availability and clinical utilization. Dual-modality imaging has advanced rapidly, primarily by incorporating the latest technological advances of CT, SPECT, and PET. Currently, combined MRI/MRSI,^{152,153} PET/CT,^{34,35} and SPECT/CT^{1,25} systems are available commercially and are used clinically. SPECT/CT systems now are available that include state-of-the-art dual-headed scintillation camera and multislice helical CT scanners for rapid patient throughput. Similarly, the PET/CT scanners now are widely available from all of the major equipment manufacturers that include high-speed helical CT scanners that offer up to 16-slice capability and submillimeter spatial resolution.^{34,35} This has reduced the time needed to acquire the transmission data from several minutes with an external radionuclide source to a few seconds with x-ray imaging. In addition, the current generation of PET/CT scanners now incorporates state-of-the-art PET detector rings, some of which operate at high count rates and can perform volumetric imaging without septa. At the time when PET/CT was first introduced clinically in 2000, PET scan times required

approximately 1 hour to complete whereas a complete PET/CT study now can be completed in the range of 10 to 15 minutes. This has led to the potential of increasing patient throughput from 3 to 4 patients a day a few years ago to 10 to 12 patients a day with current-generation PET/CT scanners.³¹ Moreover, the addition of advanced CT capability allows anatomical images to be acquired after the patient is administered with contrast media to improve lesion detection in oncologic imaging⁸⁶ or to visualize the cardiac chambers^{154,155} as well as the coronary and peripheral vasculature.^{156,157} With these capabilities, the next-generation PET/CT and SPECT/CT systems could produce high-resolution structural images of the cardiac chambers and of coronary and peripheral vasculature that can be correlated with myocardial perfusion and other functional assessments with radionuclide imaging. In addition, the use of contrast media could enable advanced radionuclide quantification techniques in clinical studies such as the template projection method discussed above.²¹ These capabilities would have the potential of improving the quantitative assessment of cancer and cardiovascular disease in comparison to studies acquired with SPECT or CT alone.

Similarly, it is expected that the technology of small animal SPECT/CT will continue to advance. Current small animal radionuclide SPECT systems obtain submillimeter spatial resolution at the cost of reduced detection efficiency. Newer multipinhole SPECT systems¹⁵⁸⁻¹⁶⁰ are under development and offer both improved geometric efficiency and spatial resolution in comparison to current radionuclide imaging approaches in a way that would improve image quality and reduce scan times for dynamic or ECG-gated cardiovascular imaging in small animals. Unfortunately, given the current state of high-resolution x-ray detectors and microfocus x-ray sources, microCT systems that allow cardiac gating and *in vivo* coronary imaging in small animals will be difficult to develop over the next few years. Nevertheless, these capabilities would be very useful for functional/structural imaging and quantitative radionuclide assessments of small animals, similar to those that we expect to develop for clinical dual-modality imaging. Finally, advances in computing power will enable the development and implementation of new anatomically-guided statistical reconstruction algorithms and data processing techniques that will offer advantages for both clinical and small animal imaging with dual-modality imaging.

While all clinical and commercial dual-modality systems have been configured in the form of PET/CT or SPECT/CT scanners, several investigators proposed and in some cases have implemented and tested prototype dual-modality systems that combine MRI with PET.^{130,161-165} The development of combined PET/MRI imaging has several important motivations.¹⁶⁶ First, MRI produces high-resolution (1 mm or better) anatomical and structural images that offer better soft-tissue contrast sensitivity than CT, has excellent contrast between white and grey matter, and is capable of assessing flow, diffusion, and cardiac motion.¹⁶⁷⁻¹⁷⁰ In addition, MRI can be combined with

magnetic resonance spectroscopy (MRS) to measure the regional biochemical content and to assess metabolic status or the presence of neoplasia and other diseases in specific tissue areas¹⁷¹⁻¹⁷³ including the prostate.^{153,174-176} Finally, MRI does not use any ionizing radiation and therefore can be used in serial studies, for paediatric cases,¹⁷⁷ and in other situations where radiation dose should be limited. Radionuclide imaging (specifically PET) records the regional distribution of radiolabeled tracers, but unlike MRS cannot distinguish the specific molecular species to which the radionuclide is attached and unlike MRI provides only little anatomical information.

There are, however, several important challenges that must be overcome in implementing and operating a combined PET/MRI or SPECT/MRI imaging system.³² In comparison to x-ray CT, MRI typically is more expensive, involves longer scan times, and produces anatomical images from which it is more difficult to derive attenuation maps for photon correction of the radionuclide data.¹⁷⁸ Furthermore, virtually all clinical radionuclide imaging detectors use photomultiplier tubes whose performance can be seriously affected in the presence of magnetic fields which are significantly smaller than those produced by modern MRI scanners. This is especially problematic in an MRI scanner which relies on rapidly switching gradient magnetic fields and radiofrequency (RF) signals to produce the magnetic resonance image. The presence of the magnetic field gradients and RF signals certainly could disrupt the performance of a photomultiplier tube and PET detector if they were located within or adjacent to the magnet of the MRI system. Similarly, the operation of the MRI system relies on a very uniform and stable magnetic field to produce the MRI image. The introduction of radiation detectors, electronics, and other bulk materials can perturb the magnetic field in a way that introduces artefacts in the MR image.

In spite of these challenges, several researchers are investigating methods to integrate a radionuclide imaging system directly in an MRI scanner. For example, it may be possible to design a radionuclide imaging system having detectors made from nonmagnetic materials that can be placed within the magnetic field of an MRI/MRS system.³² For example, Shao *et al.*^{130,179} developed a 3.8-cm ring of small scintillator crystals that was placed in the MR system for PET imaging. The crystals were optically coupled through 3 m long fiber optics to an external array of position-sensitive photomultiplier tubes, and which could be read-out through external processing electronics. By keeping the radiation-sensitive elements of the detector within the MR system, while operating the electronics away from the magnetic field, the combined system could perform simultaneous PET/MR imaging. Shao *et al.*¹⁶¹ and Slates *et al.*¹⁶² also performed simultaneous PET/MR imaging with a larger (5.6 cm-diameter) detector ring using the same design (Figure 16). Researchers at Kings College London placed the system inside of a 9.4-T NMR spectrometer to study metabolism in an isolated, perfused rat heart model. ³²P-NMR spectra were acquired simultaneously with PET images of ¹⁸F-FDG uptake in the myocardium.^{180,181} Slates *et al.*¹⁶² are

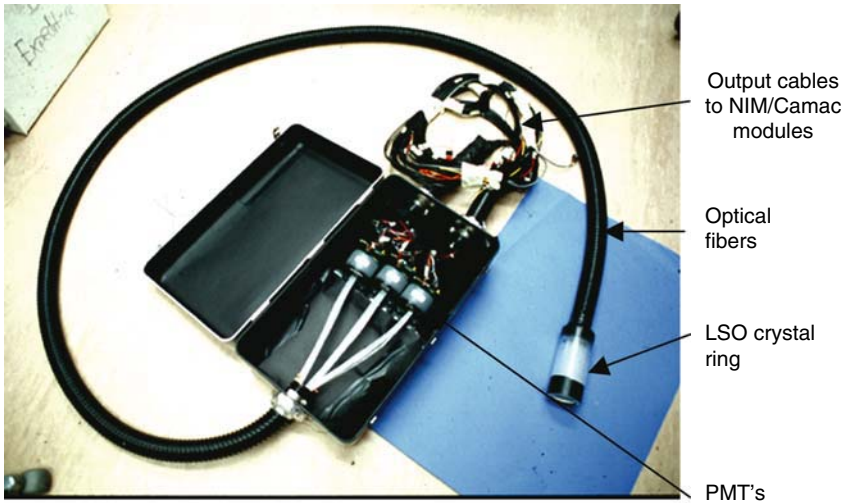


FIGURE 16. A photograph of the prototype MR compatible PET scanner (McPET) scanner developed by UCLA (CA) in collaboration with UMDS (London). Reprinted with permission from ref.¹⁷⁹

extending this design concept to develop an MR-compatible PET scanner with one ring of 480 LSO crystals arranged in 3 layers (160 crystals per layer) with a diameter of 11.2 cm corresponding to a 5 cm diameter field of view, large enough to accommodate an animal within a stereotactic frame. The system is designed to offer adequate energy resolution and sensitivity for simultaneous PET/MRI imaging of small animals (Figure 17).^{181,182}

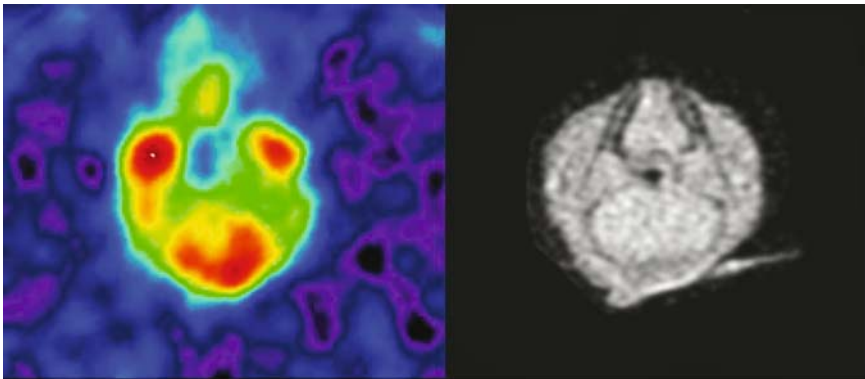


FIGURE 17. Small animal PET (left) and MRI (right) images obtained with MRI-compatible small animal PET detector (figure 16). Courtesy of Dr Simon R. Cherry (University of California, Davis) and reprinted with his permission.

Other investigators have proposed PET/MRI systems configured with suitable solid-state detectors that can be operated within a magnetic field for radionuclide imaging. For example, Pichler *et al.*¹⁸³ have tested APD's within a high-field (9.7 T) NMR spectrometer and have produced radionuclide data that appear to be free of distortion. However, it is still unknown whether the introduction of the APD's cause distortions in the magnetic field to an extent that would cause severe artefacts in the MRI image.³²

11. Concluding Remarks

Dual-modality imaging is an approach that combines imaging modalities in a way that provides diagnostic information that is not available from a single imaging modality alone. Currently available dual-modality imaging systems include SPECT/CT or PET/CT, with which the radionuclide imaging technology (SPECT or PET) provides functional or metabolic information that is complementary to anatomical information provided by CT. In addition, the development of dual-modality systems that combine radionuclide imaging with magnetic resonance imaging is an area of active research. For spatial and temporal correlation, the dual-modality data can be presented as a fused image in which the radionuclide data are displayed in colour and are superposed on the gray-scale CT image. The resulting correlated data improves differentiation of foci of radionuclide uptake that can indicate disease from those representing normal physiological uptake that are benign.

Dual-modality imaging has been available clinically since the year 2000, and as such is a relatively recent development in the fields of diagnostic radiology and nuclear medicine. However, the commercial emergence of both PET/CT and SPECT/CT has been rapid and has benefited significantly from recent technological advances in the conventional SPECT, PET, and CT. The clinical growth of dual-modality imaging has been most dramatic in the area of PET/CT which now is available from all of the major medical imaging equipment manufacturers; some observers predict that all PET systems will be installed as PET/CT scanners in the near future. Over the past year, SPECT/CT has gained increased interest and has potential clinical applications in myocardial perfusion imaging and oncologic imaging. Newer high-resolution SPECT/CT and PET/CT systems also are becoming available for small animal imaging and are needed for molecular imaging, biological research, and pharmaceutical development in small animal models of human biology and disease.

At present dual-modality imaging is primarily used for structural-functional correlations. However, as this chapter has attempted to describe, dual-modality imaging also has important ramifications for radionuclide quantification, the major theme and focus of this volume. For example, dual-modality imaging provides x-ray CT data can be normalized to obtain a patient-specific map of attenuation coefficients that be used to compensate

the correlated radionuclide data for photon attenuation or for Compton scatter. In addition, regions of interest defined anatomically on the CT image can be used to quantify the correlated radionuclide data in a way that allows more precise target and background definition, and that can use model-based methods that correct the extracted quantitative data for partial-volume effects and other perturbations. The use and understanding of dual-modality imaging as an enabling concept for radionuclide quantification is just starting to emerge. The importance of this development will only be understood and manifest over the ensuing years as PET/CT, SPECT/CT, and other forms of dual-modality imaging become available and are utilized for clinical studies of humans as well as biological investigations involving animal models of biology and disease.

References

1. Hasegawa B. H., Iwata, K., Wong, K. H. *et al.*, Dual-modality imaging of function and physiology. *Acad Radiol* **9**: 1305-1321 (2002).
2. Schiepers C. and Hoh, C. K., Positron emission tomography as a diagnostic tool in oncology. *Eur Radiol* **8**: 1481-1494 (1998).
3. Zaidi H., Quantitative SPECT: Recent developments in detector response, attenuation and scatter correction techniques. *Phys Med* **12**: 101-117 (1996).
4. Larsson A., Johansson, L., Sundstrom, T. *et al.*, A method for attenuation and scatter correction of brain SPECT based on computed tomography images. *Nucl Med Comm* **24**: 411-420 (2003).
5. Huang S. C., Hoffman, E. J., Phelps, M. E. *et al.*, Quantitation in positron emission computed tomography. 1. Effects of inaccurate attenuation correction. *J Comput Assist Tomogr* **3**: 804-814 (1979).
6. Hoffman E. J., Huang, S. C. and Phelps, M. E., Quantitation in positron emission computed tomography. I. Effect of object size. *J Comput Assist Tomogr* **3**: 299-308 (1979).
7. Tsui B., Frey, E., Zhao, X. *et al.*, The importance and implementation of accurate 3D compensation methods for quantitative SPECT. *Phys Med Biol* **39**: 509-530 (1994).
8. Tsui B. M. W., Zhao, X., Frey, E. *et al.*, Quantitative single-photon emission computed tomography: Basics and clinical considerations. *Semin Nucl Med* **24**: 38-65 (1994).
9. Rosenthal M. S., Cullom, J., Hawkins, W. *et al.*, Quantitative SPECT imaging. A review and recommendations by the focus committee of the Society of Nuclear Medicine computer and instrumentation council. *J Nucl Med* **36**: 1489-1513 (1995).
10. Zaidi H. and Hasegawa, B. H., Determination of the attenuation map in emission tomography. *J Nucl Med* **44**: 291-315 (2003).
11. Shreve P. D., Adding structure to function. *J Nucl Med* **41**: 1380-1382 (2000).
12. Schillaci O. and Simonetti, G., Fusion imaging in nuclear medicine-Applications of dual-modality systems in oncology. *Cancer Biother Radiopharm* **19**: 1-10 (2004).

13. Aizer-Dannon A., Bar-Am, A., Ron, I. G. *et al.*, Fused functional-anatomic images of metastatic cancer of cervix obtained by a combined gamma camera and an x-ray tube hybrid system with an illustrative case and review of the F-18-fluorodeoxyglucose literature. *Gynecol Oncol* **90**: 453-457 (2003).
14. Pfannenbergh A. C., Eschmann, S. M., Horger, M. *et al.*, Benefit of anatomical-functional image fusion in the diagnostic work-up of neuroendocrine neoplasms. *Eur J Nucl Med Mol Imaging* **30**: 835-843 (2003).
15. Maintz J. B. and Viergever, M. A., A survey of medical image registration. *Med Image Anal* **2**: 1-36 (1998).
16. Hutton B. F. and Braun, M., Software for image registration: algorithms, accuracy, efficacy. *Semin Nucl Med* **33**: 180-192 (2003).
17. Slomka P. J., Software approach to merging molecular with anatomic information. *J Nucl Med* **45 Suppl 1**: 36S-45S (2004).
18. Pellizzari C., Chen, G. T. Y., Spelbring, D. R. *et al.*, Accurate three-dimensional registration of CT, PET, and/or MR images of the brain. *J Comput Assist Tomogr* **13**: 20-26 (1989).
19. Pietrzyk U., Herholz, K., Fink, G. *et al.*, An interactive technique for three-dimensional image registration: validation for PET, SPECT, MRI and CT brain studies. *J Nucl Med* **35**: 2011-2018 (1994).
20. Visvikis D. and Ell, P. J., Impact of technology on the utilisation of positron emission tomography in lymphoma: current and future perspectives. *Eur J Nucl Med Mol Imaging* **30**: S106-S116 (2003).
21. Da Silva A. J., Tang, H. R., Wong, K. H. *et al.*, Absolute quantification of regional myocardial uptake of ^{99m}Tc-sestamibi with SPECT: experimental validation in a porcine model. *J Nucl Med* **42**: 772-779 (2001).
22. Blankespoor S. C., Wu, X., Kalki, K. *et al.*, Attenuation correction of SPECT using x-ray CT on an emission-transmission CT system: Myocardial perfusion assessment. *IEEE Trans Nucl Sci* **43**: 2263-2274 (1996).
23. Hasegawa B. H., Gingold, E. L., Reilly, S. M. *et al.*, Description of a simultaneous emission-transmission CT system. *Proc SPIE* Vol. 1231; pp 50-60 (1990).
24. Hasegawa B. H., Tang, H. R., Da Silva, A. J. *et al.*, Dual-modality imaging. *Nucl Instr Meth Phys Res A* **471**: 140-144 (2000).
25. Hasegawa B. H., Wong, K. H., Iwata, K. *et al.*, Dual-modality imaging of cancer with SPECT/CT. *Technol Cancer Res Treat* **1**: 449-458 (2002).
26. Lang T. F., Hasegawa, B. H., Liew, S. C. *et al.*, Description of a prototype emission-transmission CT imaging system. *J Nucl Med* **33**: 1881-1887 (1992).
27. Beyer T., Kinahan, P. E., Townsend, D. W. *et al.*, "The use of x-ray CT for attenuation correction of PET data" IEEE Nuclear Science Symposium 1577 (1994).
28. Beyer T., Townsend, D. W., Brun, T. *et al.*, A combined PET/CT scanner for clinical oncology. *J Nucl Med* **41**: 1369-1379 (2000).
29. Townsend D., Kinahan, P. and Beyer, T., Attenuation correction for a combined 3D PET/CT scanner. *Physica Medica* **12**: (Suppl 1) 43-48 (1996).
30. Townsend D. W., Beyer, T., Kinahan, P. E. *et al.*, "The SMART scanner: a combined PET/CT tomograph for clinical oncology" IEEE Nuclear Science Symposium and Medical Imaging Conference, Vol. 2; pp 1170-1174 (1998).
31. Townsend D. W., A combined PET/CT scanner: the choices. *J Nucl Med* **42**: 533-534 (2001).

32. Townsend D. W. and Cherry, S. R., Combining anatomy and function: the path to true image fusion. *Eur Radiol* **11**: 1968-1974 (2001).
33. Townsend D. W. and Beyer, T., A combined PET/CT scanner: the path to true image fusion. *Brit J Radiol* **75**: S24-S30 (2002).
34. Townsend D. W., Beyer, T. and Blodgett, T. M., PET/CT scanners: a hardware approach to image fusion. *Semin Nucl Med* **33**: 193-204 (2003).
35. Townsend D. W., Carney, J. P., Yap, J. T. *et al.*, PET/CT today and tomorrow. *J Nucl Med* **45**: Suppl 1 4S-14S (2004).
36. Vogel W. V., Oyen, W. J. G., Barentsz, J. O. *et al.*, PET/CT: Panacea, redundancy, or something in between? *J Nucl Med* **45**: 15S-24S (2004).
37. Phelps M. E., PET: The merging of biology and imaging into molecular imaging *J Nucl Med* **41**: 661-681 (2000).
38. Wahl R. L., Why nearly all PET of abdominal and pelvic cancers will be performed as PET/CT. *J Nucl Med* **45**: 82S-95S (2004).
39. Goerres G. W., von Schulthess, G. K. and Steinert, H. C., Why most PET of lung and head-and-neck cancer will be PET/CT. *J Nucl Med* **45**: 66S-71S (2004).
40. Even-Sapir E., Keidar, Z., Sachs, J. *et al.*, The new technology of combined transmission and emission tomography in evaluation of endocrine neoplasms. *J Nucl Med* **42**: 998-1004 (2001).
41. Israel O., Keidar, Z., Iosilevsky, G. *et al.*, The fusion of anatomic and physiologic imaging in the management of patients with cancer. *Semin Nucl Med* **31**: 191-205 (2001).
42. Tang H. R., "A Combined X-ray CT-Scintillation Camera System for Measuring Radionuclide Uptake in Tumors," Ph.D Thesis, University of California, 1998.
43. Kinahan P. E., Townsend, D. W., Beyer, T. *et al.*, Attenuation correction for a combined 3D PET/CT scanner. *Med Phys* **25**: 2046-2053 (1998).
44. Kinahan P. E., Hasegawa, B. H. and Beyer, T., X-ray-based attenuation correction for position tomography/computed tomography scanners. *Semin Nucl Med* **33**: 166-179 (2003).
45. Mayneord W. V., The radiology of the human body with radioactive isotopes. *Brit J Radiol* **25**: 517-525 (1952).
46. Mayneord W. V., Radiological research. *Brit J Radiol* **27**: 309-317 (1954).
47. Mayneord W. V., Evans, H. D. and Newberry, S. P., An instrument for the formation of visual images of ionizing radiations. *J Scient Instruments* **32**: 45-50 (1955).
48. Anger H. O., Whole-body scanner Mark II. *J Nucl Med* **7**: 331-332 (1966).
49. Anger H. O. and McRae, J., Transmission scintiphotography. *J Nucl Med* **9**: 267-269 (1968).
50. Cameron J. R. and Sorenson, J., Measurement of bone mineral *in vivo*: an improved method. *Science* **142**: 230-232 (1963).
51. Kuhl D. E., Hale, J. and Eaton, W. L., Transmission scanning: A useful adjunct to conventional emission scanning for accurately keying isotope deposition to radiographic anatomy. *Radiology* **87**: 278-284 (1966).
52. Kuhl D. E., Edwards, R. O., Ricci, A. R. *et al.*, The Mark IV system for radionuclide computed tomography of the brain. *Radiology* **121**: 405-413 (1976).
53. Budinger T. F. and Gullberg, G. T., Three-dimensional reconstruction in nuclear medicine emission imaging. *IEEE Trans Nucl Sci* **NS-21**: 2-20 (1974).
54. Mirshanov D. M., Transmission-Emission Computer Tomograph, USSR Patent 621.386:616-073 20.01.87-SU-181935 (January 20, 1987).

55. Kaplan C. H., Transmission/emission registered image (TERI) computed tomography scanners, International patent application No. PCT/US90/03722 (1989).
56. Hasegawa B. H., Tang, H. R., Iwata, K. *et al.*, Correlation of structure and function with dual modality imaging. *Physica Medica* **17**: 241-248 (2001).
57. Hasegawa B. H., Reilly, S. M., Gingold, E. L. *et al.*, Design considerations for a simultaneous emission-transmission CT scanner. [abstract] *Radiology* **173(P)**: 414 (1989).
58. Lang T. F., Hasegawa, B. H., Liew, S. C. *et al.*, "A prototype emission-transmission imaging system" IEEE Nuclear Science Symposium and Medical Imaging Conference, Santa Fe, NM, Vol. 3; pp 1902-1906 (1991).
59. Kalki K., Blankespoor, S. C., Brown, J. K. *et al.*, Myocardial perfusion imaging with a combined x-ray CT and SPECT system. *J Nucl Med* **38**: 1535-1540 (1997).
60. Kalki K., Heanue, J. A., Blankespoor, S. C. *et al.*, A combined SPECT and CT medical imaging system. *Proc SPIE* Vol. 2432; pp 367-375 (1995).
61. Cohade C., Osman, M. M., Leal, J. *et al.*, Direct comparison of F-18-FDG PET and PET/CT in patients with colorectal carcinoma. *J Nucl Med* **44**: 1797-1803 (2003).
62. Fricke H., Fricke, E., Weise, R. *et al.*, A method to remove artifacts in attenuation-corrected myocardial perfusion SPECT Introduced by misalignment between emission scan and CT-derived attenuation maps. *J Nucl Med* **45**: 1619-1625 (2004).
63. Takahashi Y., Murase, K., Higashino, H. *et al.*, Attenuation correction of myocardial SPECT images with X-ray CT: effects of registration errors between X-ray CT and SPECT. *Ann Nucl Med* **16**: 431-435 (2002).
64. Blankespoor S. C., "Attenuation correction of SPECT using x-ray CT for myocardial perfusion assessment," Master's thesis, University of California, 1996.
65. Koral K. F., Dewaraja, Y., Li, J. *et al.*, Update on hybrid conjugate-view SPECT tumor dosimetry and response in ^{131}I -tositumomab therapy of previously untreated lymphoma patients. *J Nucl Med* **44**: 457-464 (2003).
66. Keidar Z., Israel, O. and Krausz, Y., SPECT/CT in tumor imaging? technical aspects and clinical applications. *Semin Nucl Med* **33**: 205-218 (2003).
67. Even-Sapir E., Lerman, H., Lievshitz, G. *et al.*, Lymphoscintigraphy for sentinel node mapping using a hybrid SPECT/CT system. *J Nucl Med* **44**: 1413-1420 (2003).
68. Israel O., Mor, M., Gaitini, D. *et al.*, Combined functional and structural evaluation of cancer patients with a hybrid camera-based PET/CT system using F-18 FDG. *J Nucl Med* **43**: 1129-1136 (2002).
69. Tang H. R., Da Silva, A. J., Matthay, K. K. *et al.*, Neuroblastoma imaging using a combined CT scanner-scintillation camera and I-131 MIBG. *J Nucl Med* **42**: 237-247 (2001).
70. Bocher M., Balan, A., Krausz, Y. *et al.*, Gamma camera-mounted anatomical x-ray tomography: technology, system characteristics, and first images. *Eur J Nucl Med* **27**: 619-627 (2000).
71. Liu Y., Wackers, F. J., Natale, D. *et al.*, Validation of a hybrid SPECT/CT system with attenuation correction: A phantom study and multicenter trial. [abstract] *J Nucl Med* **44**: 209P (2003).
72. Rajasekar D., Datta, N. R., Gupta, R. K. *et al.*, Multimodality image fusion in dose escalation studies in brain tumors. *J Appl Clin Med Phys* **4**: 8-16 (2003).

73. Schoder H., Larson, S. M. and Yeung, H. W. D., PET/CT in oncology: Integration into clinical management of lymphoma, melanoma, and gastrointestinal malignancies. *J Nucl Med* **45**: 72S-81S (2004).
74. Cook G. J. R. and Ott, R. J., Dual-modality imaging. *Eur Radiol* **11**: 1857-1858 (2001).
75. Chang L. T., A method for attenuation correction in radionuclide computed tomography. *IEEE Trans Nucl Sci* **NS-25**: 638-643 (1978).
76. Harris C. C., Greer, K. L., Jaszczak, R. J. *et al.*, Tc-99m attenuation coefficients in water-filled phantoms determined with gamma cameras. *Med Phys* **11**: 681-685 (1985).
77. Malko J. A., Van Heertum, R. L., Gullberg, G. T. *et al.*, SPECT liver imaging using an iterative attenuation correction algorithm and an external flood source. *J Nucl Med* **27**: 701-705 (1986).
78. Thompson C. J., Ranger, N. T. and Evans, A. C., Simultaneous transmission and emission scans in positron emission tomography. *IEEE Trans Nucl Sci* **36**: (1989).
79. Tsui B. M. W., Hu, H. B., Gilland, D. R. *et al.*, Implementation of simultaneous attenuation and detector response correction in SPECT *IEEE Trans Nucl Sci* **NS-35**: 778-783 (1988).
80. Tsui B. M. W., Gullberg, G. T., Edgerton, E. R. *et al.*, Correction of nonuniform attenuation in cardiac SPECT imaging *J Nucl Med* **30**: 497-507 (1989).
81. Blankespoor S., Wu, X., Kalki, K. *et al.*, "Attenuation correction of SPECT using x-ray CT on an emission-transmission CT system" IEEE Nuclear Science Symposium and Medical Imaging Conference, Vol. 2; pp 1126-1130 (1995).
82. LaCroix K. J., "An investigation of the use of single-energy x-ray CT images for attenuation compensation in SPECT," Master's thesis, University of North Carolina at Chapel Hill, 1994.
83. Perring S., Summers, Q., Fleming, J. *et al.*, A new method of quantification of the pulmonary regional distribution of aerosols using combined CT and SPECT and its application to nedocromil sodium administered by metered dose inhaler. *Br J Radiol* **67**: 46-53 (1994).
84. Gullberg G. T., Huesman, R. H., Malko, J. A. *et al.*, An attenuated projector-backprojector for iterative SPECT reconstruction. *Phys Med Biol* **30**: 799-816 (1985).
85. Ficaro E. P. and Wackers, F. J., Should SPET attenuation correction be more widely employed in routine clinical practice? *Eur J Nucl Med* **29**: 409-412 (2002).
86. Antoch G., Freudenberg, L. S., Beyer, T. *et al.*, To enhance or not to enhance: [F-18]-FDG and CT contrast agents in dual-modality [F-18]-FDG PET/CT. *J Nucl Med* **45**: 56S-65S (2004).
87. Carney J. P., Beyer, T., Brasse, D. *et al.*, Clinical PET/CT using oral CT contrast agents. [abstract] *J Nucl Med* **44**: 272P (2002).
88. Mukai T., Links, J. M., Douglass, K. H. *et al.*, Scatter correction in SPECT using non-uniform attenuation data. *Phys Med Biol* **33**: 1129-1140 (1988).
89. Kessler R. M., Ellis, J. R. and Eden, M., Analysis of emission tomographic scan data: Limitations imposed by resolution and background. *J Comput Assist Tomogr* **8**: 514-522 (1984).
90. Tang H. R., Brown, J. K. and Hasegawa, B. H., Use of x-ray CT-defined regions of interest for the determination of SPECT recovery coefficients. *IEEE Trans Nucl Sci* **44**: 1594-1599 (1997).

91. Koole M., Laere, K. V., de Walle, R. V. *et al.*, MRI guided segmentation and quantification of SPECT images of the basal ganglia: a phantom study. *Comput Med Imaging Graph* **25**: 165-172 (2001).
92. Rousset O. G., Ma, Y. and Evans, A. C., Correction for partial volume effects in PET: principle and validation. *J Nucl Med* **39**: 904-911 (1998).
93. Meltzer C. C., Kinahan, P. E., Greer, P. J. *et al.*, Comparative evaluation of MR-based partial-volume correction schemes for PET. *J Nucl Med* **40**: 2053-2065 (1999).
94. Koral K. F., Li, J., Dewaraja, Y. *et al.*, I-131 anti-B1 therapy/tracer uptake ratio using a new procedure for fusion of tracer images to computed tomography images. *Clin Cancer Res* **5**: 3004s-3009s (1999).
95. Koral K. F., Dewaraja, Y., Clarke, L. A. *et al.*, Tumor-absorbed-dose estimates versus response in tositumomab therapy of previously untreated patients with follicular non-Hodgkin's lymphoma: preliminary report. *Cancer Biother Radiopharm* **15**: 347-355 (2000).
96. Formiconi A. R., Least squares algorithm for region-of-interest evaluation in emission tomography. *IEEE Trans Med Imag* **12**: 90-100 (1993).
97. Liu A., Williams, L. E. and Raubitschek, A. A., A CT assisted method for absolute quantitation of internal radioactivity. *Med Phys* **23**: 1919-1228 (1996).
98. Carson R. E., A maximum likelihood method for region-of-interest evaluation in emission tomography. *J Comput Assist Tomogr* **100**: 654-663 (1986).
99. Koral K. F., Zasadny, K. R., Kessler, M. L. *et al.*, CT-SPECT fusion plus conjugate views for determining dosimetry in iodine-131-monoclonal antibody therapy of lymphoma patients. *J Nucl Med* **35**: 1714-1720 (1994).
100. Koral K. F., Lin, S., Fessler, J. A. *et al.*, Preliminary results from intensity-based CT-SPECT fusion in I-131 anti-B1 monoclonal-antibody therapy of lymphoma. *Cancer* **80**: 2538-2544 (1997).
101. Koral K. F., Dewaraja, Y., Li, J. *et al.*, Initial results for hybrid SPECT - conjugate-view tumor dosimetry in ¹³¹I-anti-B1 antibody therapy of previously untreated patients with lymphoma. *J Nucl Med* **41**: 1579-1586 (2000).
102. Koral K. F., Francis, I. R., Kroll, S. *et al.*, Volume reduction versus radiation dose for tumors in previously untreated lymphoma patients who received iodine-131 tositumomab therapy. Conjugate views compared with a hybrid method. *Cancer* **94**: 1258-1263 (2002).
103. Koral K. F., Kaminski, M. S. and Wahl, R. L., Correlation of tumor radiation-absorbed dose with response is easier to find in previously untreated patients. *J Nucl Med* **44**: 1541-1543 (2003).
104. Koral K. F., Zaidi, H. and Ljungberg, M., "Medical imaging techniques for radiation dosimetry" in: *Therapeutic applications of Monte Carlo calculations in nuclear medicine*, edited by H Zaidi and G Sgouros Institute of Physics Publishing, Bristol, (2002), pp 55-83.
105. Patton J. A., Delbeke, D. and Sandler, M. P., Image fusion using an integrated, dual-head coincidence camera with x-ray tube-based attenuation maps. *J Nucl Med* **41**: 1364-1368 (2000).
106. Ratib O., PET/CT image navigation and communication. *J Nucl Med* **45**: 46S-55S (2004).
107. Steinert H. C. and von Schulthess, G. K., Initial clinical experience using a new integrated in-line PET/CT system. *Br J Radiol* **73**: S36-S38 (2002).

108. Beyer T., Antoch, G., Muller, S. *et al.*, Acquisition protocol considerations for combined PET/CT imaging. *J Nucl Med* **45**: 25S-35S (2004).
109. Bar-Shalom R., Yefemov, N., Guralnik, L. *et al.*, Clinical performance of PET/CT in evaluation of cancer: Additional value for diagnostic imaging and patient management. *J Nucl Med* **44**: 1200-1209 (2003).
110. Cohade C. and Wahl, R. L., Applications of positron emission tomography/computed tomography image fusion in clinical positron emission tomography - clinical use, interpretation, methods, diagnostic improvements. *Semin Nucl Med* **33**: 228-237 (2003).
111. Cherry S. R., In vivo molecular and genomic imaging: new challenges for imaging physics. *Phys Med Biol* **49**: R13-R48 (2004).
112. Weissleder R. and Mahmood, U., Molecular imaging. *Radiology* **219**: 316-333 (2001).
113. Hanahan D., Transgenic mice as probes into complex systems. *Science* **246**: 1265-1275 (1989).
114. Sigmund C. D., Major approaches for generating and analyzing transgenic mice. *Hypertension* **22**: 599-607 (1993).
115. Wight D. C. and Wagner, T. E., Transgenic mice: a decade of progress in technology and research. *Mutation Res* **307**: 429-440 (1994).
116. James J. F., Hewett, T. E. and Robbins, J., Cardiac physiology in transgenic mice. *Circ Res* **82**: 407-415 (1998).
117. Wu M. C., Gao, D. W., Sievers, R. E. *et al.*, Pinhole single-photon emission computed tomography for myocardial perfusion imaging of mice. *J Am Coll Cardiol* **42**: 576-582 (2003).
118. Paulus M. J., Sari-Sarraf, H., Bleason, S. S. *et al.*, A new x-ray computed tomography system for laboratory mouse imaging. *IEEE Trans Nucl Sci* **46**: 558-564 (1999).
119. Cherry S. R., Shao, Y., Silverman, R. W. *et al.*, MicroPET: a high resolution PET scanner for imaging small animals. *IEEE Trans Nucl Sci* **44**: 1161-1166 (1997).
120. Hasegawa B. H., Wu, M. C., Iwata, K. *et al.*, Applications of penetrating radiation for small animal imaging. *Proc SPIE* Vol. 4786; pp 80-90 (2002).
121. Paulus M. J., Gleason, S. S., Kennel, S. J. *et al.*, High resolution X-ray computed tomography: an emerging tool for small animal cancer research. *Neoplasia* **2**: 62-70 (2000).
122. Kennel S. J., Davis, I. A., Branning, J. *et al.*, High resolution computed tomography and MRI for monitoring lung tumor growth in mice undergoing radioimmunotherapy: correlation with histology. *Med Phys* **27**: 1101-1107 (2000).
123. Paulus M. J., Gleason, S. S., Easterly, M. E. *et al.*, A review of high-resolution X-ray computed tomography and other imaging modalities for small animal research. *Lab Anim (NY)* **30**: 36-45 (2001).
124. Ishizu K., Mukai, T., Yonekura, Y. *et al.*, Ultra-high resolution SPECT system using four pinhole collimators for small animal studies. *J Nucl Med* **36**: 2282-2286 (1995).
125. Jaszczak R. J., Li, J., Wang, H. *et al.*, Pinhole collimation for ultra high-resolution, small field of view SPECT. *Phys Med Biol* **39**: 425-437 (1994).
126. MacDonald L. R., Patt, B. E., Iwanczyk, J. S. *et al.*, Pinhole SPECT of mice using the LumaGEM gamma camera. *IEEE Trans Nucl Sci* **48**: 830-836 (2001).

127. Ogawa K., Kawade, T., Nakamura, K. *et al.*, Ultra high resolution pinhole SPECT for small animal study. *IEEE Trans Nucl Sci* **45**: 3122-3126 (1998).
128. Wu M. C., Hasegawa, B. H. and Dae, M. W., Performance evaluation of a pinhole SPECT system for myocardial perfusion imaging of mice. *Med Phys* **29**: 2830-2839 (2002).
129. Weber D. A. and Ivanovic, M., Pinhole SPECT: ultra-high resolution imaging for small animal studies. *J Nucl Med* **36**: 2287-2289 (1995).
130. Shao Y., Cherry, S. R., Farahani, K. *et al.*, Simultaneous PET and MR imaging. *Phys Med Biol* **42**: 1965-1970 (1997).
131. Goertzen A. L., Meadors, A. K., Silverman, R. W. *et al.*, Simultaneous molecular and anatomical imaging of the mouse *in vivo*. *Phys Med Biol* **21**: 4315-4328 (2002).
132. Weisenberger A. G., Wojcik, R., Bradley, E. L. *et al.*, SPECT-CT system for small animal imaging. *IEEE Trans Nucl Sci* **50**: 74-79 (2003).
133. Williams M. B., Zhang, G., More, M. J. *et al.*, Integrated CT-SPECT system for small animal imaging. *Proc SPIE* Vol. 4142; pp 265-274 (2000).
134. Welsh R. E., Brewer, P., Bradley, E. L. *et al.*, "An economical dual-modality small animal imaging system with application to studies of diabetes" IEEE Nuclear Science Symposium and Medical Imaging Conference Record, Vol. 3; pp 1845-1848 (2002).
135. Kastis G. A., Furenlid, L. R., Wilson, D. W. *et al.*, Compact CT/SPECT small-animal imaging system. *IEEE Trans Nucl Sci* **51**: 63-67 (2004).
136. Iwata K., Wu, M. C. and Hasegawa, B. H., "Design of combined x-ray CT and SPECT systems for small animals" IEEE Nuclear Science Symposium and Medical Imaging Conference Record, Vol. 3; pp 1608-1612 (1999).
137. Iwata K., Hwang, A. B., Wu, M. C. *et al.*, "Design and utility of a small animal CT/SPECT system" IEEE Nuclear Science Symposium and Medical Imaging Conference Record, Vol. 3; pp 1849-1852 (2002).
138. MacDonald L. R., Iwata, K., Patt, B. E. *et al.*, Evaluation of x-ray detectors for dual-modality CT-SPECT animal imaging. *Proc SPIE* Vol. 4786; pp 91-102 (2002).
139. Andre M. P., Spivey, B. A., Martin, P. J. *et al.*, Integrated CMOS-selenium x-ray detector for digital mammography. *Proc SPIE* Vol. 3336; pp 204-209 (1998).
140. Song X., Frey, E. C. and Tsui, B. M. W., "Development and evaluation of a microCT system for small animal imaging" IEEE Nuclear Science Symposium and Medical Imaging Conference Record, Vol. 3; pp 1600-1604 (2002).
141. Hwang A. B., Iwata, K., Sakdinawat, A. E. *et al.*, "Gantry specifications for a dual modality imaging system for small animals" IEEE Nuclear Science Symposium and Medical Imaging Conference Record, Vol. 2; pp 1303-1307 (2003).
142. Varady P., Li, J. Z., Alden, T. D. *et al.*, CT and radionuclide study of BMP-2 gene therapy-induced bone formation. *Acad Radiol* **9**: 632-637 (2002).
143. MacDonald L. R., Iwanczyk, J. S., Patt, B. E. *et al.*, "Development of new high resolution detectors for small animal SPECT imaging" IEEE Nuclear Science Symposium and Medical Imaging Conference Record, Vol. 3; pp 21/75 (2002).
144. McElroy D. P., MacDonald, L. R., Beekman, F. J. *et al.*, Performance evaluation of A-SPECT: A high resolution desktop pinhole SPECT system for imaging small animals. *IEEE Trans Nucl Sci* **49**: 2139-2147 (2002).

145. Yazaki P. J., Shively, L., Clark, C. *et al.*, Mammalian expression and hollow fiber bioreactor production of recombinant anti-CEA diabody and minibody for clinical applications. *J Immun Methods* **253**: 195-208 (2001).
146. Hasegawa B. H., Barber, W. C., Funk, T. *et al.*, Implementation and applications of dual-modality imaging. *Nucl Instr Meth Phys Res A* **525**: 236-241 (2004).
147. Weber D. A. and Ivanovic, M., Ultra-high-resolution imaging of small animals: implications for preclinical and research studies. *J Nucl Cardiol* **6**: 332-344 (1999).
148. Paulino A. C., Thorstad, W. L. and Fox, T., Role of fusion in radiotherapy treatment planning *Semin Nucl Med* **33**: 238-243 (2003).
149. Munley M. T., Marks, L. B., Scarfone, C. *et al.*, Multimodality nuclear medicine imaging in three-dimensional radiation treatment planning for lung cancer: challenges and prospects. *Lung Cancer* **23**: 105-14 (1999).
150. Osman M. M., Cohade, C., Nakamoto, Y. *et al.*, Clinically significant inaccurate localization of lesions with PET/CT: frequency in 300 patients. *J Nucl Med* **44**: 240-243 (2003).
151. Nahmias C., Nutt, R., Hichwa, R. D. *et al.*, PET tomograph designed for five minute routine whole body studies. [abstract] *J Nucl Med* **43**: 11P (2002).
152. Nelson S. J., Vigneron, D. B. and Dillon, W. P., Serial evaluation of patients with brain tumors using volume MRI and 3D ^1H MRSI. *NMR Biomed* **12**: 123-138 (1999).
153. Kurhanewicz J., Swanson, M. G., Nelson, S. J. *et al.*, Combined magnetic resonance imaging and spectroscopic imaging approach to molecular imaging of prostate cancer. *J Magn Reson Imaging* **16**: 451-463 (2002).
154. Bost L. M., Lipton, M. J., Kwong, R. Y. *et al.*, Computed tomography for assessment of cardiac chambers, valves, myocardium and pericardium. *Cardiol Clin* **21**: 561-585 (2003).
155. Chan F. P., Cardiac multidetector-row computed tomography: principles and applications. *Semin Roentgenol* **38**: 294-302 (2003).
156. Nieman K., Rensing, B., Munne, A. *et al.*, Three-dimensional coronary anatomy in contrast-enhanced multislice computed tomography. *Prev Cardiol* **5**: 79-83 (2002).
157. Foley W. D. and Karcaaltincaba, M., Computed tomography angiography: Principles and clinical applications. *J Comput Assist Tomogr* **27**: S23-S30 (2003).
158. Peterson T. F., Kim, H., Crawford, M. J. *et al.*, "SemiSPECT: A small-animal imaging system based on eight CdZnTe pixel detectors" IEEE Nuclear Science Symposium and Medical Imaging Conference Record, Vol. 3; pp 1844-1847 (2003).
159. Liu Z., Kastis, G. A., Stevenson, G. D. *et al.*, Quantitative analysis of acute myocardial infarct in rat hearts with ischemia-reperfusion using a high-resolution stationary SPECT system. *J Nucl Med* **43**: 933-939 (2002).
160. Schramm N. U., Ebel, G., Engeland, U. *et al.*, High-resolution SPECT using multipinhole collimation. *IEEE Trans Nucl Sci* **50**: 315-320 (2003).
161. Shao Y., Cherry, S. R., Farahani, K. *et al.*, Development of a PET detector system compatible with MRI/NMR systems. *IEEE Trans Nucl Sci* **44**: 1167-1171 (1997).
162. Slates R., Cherry, S. R., Boutefnouchet, A. *et al.*, Design of a small animal MR compatible PET scanner. *IEEE Trans Nucl Sci* **46**: 565-570 (1999).

163. Christensen N. L., Hammer, B. E., Heil, B. G. *et al.*, Positron emission tomography within a magnetic field using photomultiplier tubes and light-guides. *Phys Med Biol* **40**: 691-697 (1995).
164. Hammer B. E., Christensen, N. L. and Heil, B. G., Use of a magnetic field to increase the spatial resolution of positron emission tomography. *Med Phys* **21**: 1917-1920 (1994).
165. Mackewn J. E., Strul, D., Hallett, W. A. *et al.*, "Design and development of an MR-compatible PET scanner for imaging small animals" IEEE Nuclear Science Symposium and Medical Imaging Conference, Rome, Italy, (2004) *in press*
166. Gaa J., Rummeny, E. J. and Seemann, M. D., Whole-body imaging with PET/MRI. *Eur J Med Res* **30**: 309-312 (2004).
167. Maronpot R. R., Sills, R. C. and Johnson, G. A., Applications of magnetic resonance microscopy. *Toxicol Pathol* **32**: 42-48 (2004).
168. Johnson G. A., Cofer, G. P., Gewalt, S. L. *et al.*, Morphologic phenotyping with MR microscopy: the visible mouse. *Radiology* **222**: 789-793 (2002).
169. Hu X. and Norris, D. G., Advances in high-field magnetic resonance imaging. *Annu Rev Biomed Eng* **6**: 157-184 (2004).
170. Lima J. A. and Desai, M. Y., Cardiovascular magnetic resonance imaging: current and emerging applications. *J Am Coll Cardiol* **15**: 1164-1171 (2004).
171. Hasumi M., Suzuki, K., Taketomi, A. *et al.*, The combination of multi-voxel MR spectroscopy with MR imaging improve the diagnostic accuracy for localization of prostate cancer. *Anticancer Res* **23**: 4223-4227 (2003).
172. Yeung D. K., Yang, W. T. and Tse, G. M., Breast cancer: in vivo proton MR spectroscopy in the characterization of histopathologic subtypes and preliminary observations in axillary node metastases. *Radiology* **225**: 190-197 (2002).
173. Turner D. A., MR spectroscopy and imaging of breast cancer. A brief history. *Magn Reson Imaging Clin N Am* **2**: 505-510 (1994).
174. Coakley F. V., Teh, H. S., Qayyum, A. *et al.*, Endorectal MR imaging and MR spectroscopic imaging for locally recurrent prostate cancer after external beam radiation therapy: preliminary experience. *Radiology* **233**: 441-448 (2004).
175. Coakley F. V., Qayyum, A. and Kurhanewicz, J., Magnetic resonance imaging and spectroscopic imaging of prostate cancer. *J Urol* **170**: S69-75; discussion S75-76 (2003).
176. Swanson M. G., Vigneron, D. B., Tran, T. K. *et al.*, Magnetic resonance imaging and spectroscopic imaging of prostate cancer. *Cancer Invest* **19**: 510-523 (2001).
177. Vick G. W., Recent advances in pediatric cardiovascular MRI. *Curr Opin Pediatr* **15**: 454-462 (2003).
178. Zaidi H., Montandon, M.-L. and Slosman, D. O., Magnetic resonance imaging-guided attenuation and scatter corrections in three-dimensional brain positron emission tomography. *Med Phys* **30**: 937-948 (2003).
179. Slates R., Farahani, K., Shao, Y. *et al.*, A study of artefacts in simultaneous PET and MR imaging using a prototype MR compatible PET scanner. *Phys Med Biol* **44**: 2015-2027 (1999).
180. Garlick P. B., Marsden, P. K., Cave, A. C. *et al.*, PET and NMR dual acquisition (PANDA): Applications to isolated perfused rat hearts. *NMR Biomed* **10**: 138-142 (1997).
181. Garlick P. B., Simultaneous PET and NMR-Initial results from isolated, perfused rat hearts. *Br J Radiol* 75 Spec No: S60-66 (2002).

182. Marsden P. K., Strul, D., Keevil, S. F. *et al.*, Simultaneous PET and NMR. *Br J Radiol* 75 Spec No: S53-59 (2002).
183. Pichler B., Lorenz, E., Mirzoyan, R. *et al.*, “Performance tests of a LSO-APD PET module in a 9.4 Tesla magnet” IEEE Nuclear Science Symposium and Medical Imaging Conference Record, Vol. 2; *pp* 1237-1239 (1997).

Quantitative Analysis in Nuclear Medicine Imaging

Zaidi, H. (Ed.)

2006, XI, 583 p. 166 illus., 56 illus. in color., Hardcover

ISBN: 978-0-387-23854-8